ORIGINAL ARTICLE

WILEY | Development, Growth & Differentiation

Hoxa13 regulates expression of common Hox target genes involved in cartilage development to coordinate the expansion of the autopodal anlage

Shiori Yamamoto[1] | Yuji Uchida[1] | Tomomi Ohtani[1] | Erina Nozaki[1] | Chunyang Yin[1] | Yoshihiro Gotoh[1] | Nayuta Yakushiji-Kaminatsui[2] | Tetsuya Higashiyama[1,3] | Takamasa Suzuki[4] | Tatsuya Takemoto[5] | Yo-ichi Shiraishi[1] | Atsushi Kuroiwa[1] (iD)

[1]Division of Biological Science, Graduate School of Science, Nagoya University, Nagoya-shi, Aichi-ken, Japan

[2]School of Life Sciences, Federal Institute of Technology, Lausanne, Lausanne, Switzerland

[3]Institute of Transformative Bio-Molecules (WPI-ITbM), Nagoya University, Nagoya-shi, Aichi-ken, Japan

[4]Department of Biological Chemistry, College of Bioscience and Biotechnology, Chubu University, Kasugai-shi, Aichi-ken, Japan

[5]Laboratory for Embryology, Institute for Advanced Medical Sciences, Tokushima University, Tokushima, Japan

Correspondence
Yo-ichi Shiraishi and Atsushi Kuroiwa, Division of Biological Science, Graduate School of Science, Nagoya University, Nagoya-shi, Aichi-ken, Japan.
Emails: shiraishi.yo-ichi@h.mbox.nagoya-u.ac.jp;akuro@bio.nagoya-u.ac.jp

To elucidate the role of Hox genes in limb cartilage development, we identified the target genes of HOXA11 and HOXA13 by ChIP-Seq. The ChIP DNA fragment contained evolutionarily conserved sequences and multiple highly conserved HOX binding sites. A substantial portion of the HOXA11 ChIP fragment overlapped with the HOXA13 ChIP fragment indicating that both factors share common targets. Deletion of the target regions neighboring Bmp2 or Tshz2 reduced their expression in the autopod suggesting that they function as the limb bud-specific enhancers. We identified the Hox downstream genes as exhibiting expression changes in the Hoxa13 knock out (KO) and Hoxd11-13 deletion double mutant (Hox13 dKO) autopod by Genechip analysis. The Hox downstream genes neighboring the ChIP fragment were defined as the direct targets of Hox. We analyzed the spatial expression pattern of the Hox target genes that encode two different categories of transcription factors during autopod development and Hox13dKO limb bud. (a) Bcl11a, encoding a repressor of cartilage differentiation, was expressed in the E11.5 autopod and was substantially reduced in the Hox13dKO. (b) The transcription factors Aff3, Bnc2, Nfib and Runx1t1 were expressed in the zeugopodal cartilage but not in the autopod due to the repressive or relatively weak transcriptional activity of Hox13 at E11.5. Interestingly, the expression of these genes was later observed in the autopodal cartilage at E12.5. These results indicate that Hox13 transiently suspends the cartilage differentiation in the autopodal anlage

---

Abbreviations: ChIP, Chromatin immunoprecipitation; ChIP-Seq, ChIP-sequencing; HBS, HOX binding sequence; KO, knock out; PCR, polymerase chain reaction.

---

via multiple pathways until establishing the paddle-shaped structure required to generate five digits.

KEYWORDS

autopod, cartilage, ChIP-Seq, Hoxa11, Hoxa13, limb, target gene

1 | INTRODUCTION

The tetrapod free limb is subdivided into three anatomical domains along the proximodistal axis: the stylopod, zeugopod and autopod. These domains possess a specific number and pattern of the bones and each bone possesses a unique morphology and length. During limb development, the mesenchymal cells of the limb bud first form precartilaginous aggregates, which eventually grow and differentiate into the limb cartilage (Gilbert & Barresi, 2016). The process occurs sequentially in the proximal to distal direction with the growth of the limb bud. Expression of *Hox* genes belonging to the *Abd-B* family, *Hox9-13*, is closely related to the anatomical domains of the limb bones (Izpisua-Belmonte, Tickle, Dolle, Wolpert, & Duboule, 1991; Yokouchi, Sasaki, & Kuroiwa, 1991) and crucial for controlling morphogenesis and patterning of the limb cartilage (Pineault & Wellik, 2014). *Hoxa11* and *Hoxd11* show overlapping expression in the zeugopodal mesenchyme and simultaneous loss of function of both genes in the forelimb bud results severe truncation of the zeugopodal bones without affecting the other long bones (Boulet & Capecchi, 2004; Davis, Witte, Hsieh-Li, Potter, & Capecchi, 1995). *Hoxa13* and *Hoxd13* are expressed in the autopodal mesenchyme and double knockout (KO) mice have smaller autopods during the embryonic stage and there was almost no sign of cartilage patterning in the entire autopod (Fromental-Ramain et al., 1996). These double homozygous KO mice exhibited much more severe phenotypes than single homozygous KOs suggesting that the paralogous genes are functionally redundant (Davis et al., 1995; Fromental-Ramain et al., 1996). A further role for *Hox* in domain-specific cartilage development was shown by misexpression of *Hox* in the limb mesenchyme. Viral or genetic misexpression of *Hoxa13* or *Hoxd13* in the zeugopodal mesenchyme repressed cartilage differentiation and proliferation resulting in zeugopod-specific cartilage truncation (Goff & Tabin, 1997; Peichel, Prabhakaran, & Vogt, 1997; Yokouchi et al., 1995). Thus, *Hox* genes are expressed in a domain-specific manner in the limb bud mesenchyme and have a crucial function in domain-specific cartilage morphogenesis. Since *Hox* encodes a transcription factor, *Hox* target genes function in region/compartment-specific formation of the precartilaginous condensation, cellular differentiation and proliferation of the cartilage.

In contrast, *Hox* genes also control the expression of *Fgf10* in the distal limb mesenchyme and *Shh* in the posterior mesenchyme to regulate limb outgrowth and proper supply of mesenchymal cells in coordination with the developmental time course of the limb bud (Capellini et al., 2006; Kmita et al., 2005; Sheth et al., 2013). How this growth control system coordinates with the domain-specific cartilage pattern formation system is an important question that remains to be resolved.

In order to understand the system that determines domain-specific limb cartilage development, it is essential to identify the direct *Hox* target genes. While limited numbers of *Hox* downstream genes have been reported, the known function of these genes does not sufficiently explain the *Hox* loss-of-function phenotype (McCabe & Innis, 2005; Salsi & Zappavigna, 2006). Recently the *Hox* target genes in the limb bud were exhaustively identified by ChIP-Seq analysis, which opened the door to elucidate the function of the *Hox* genes in region-specific cartilage development (Jerkovic et al., 2017; Sheth et al., 2016). Since *Hox11* and *Hox13* control the growth and cartilage differentiation of the zeugopod and autopod, respectively, we raised questions if they share common targets, and if so, how the common targets are differentially regulated to give rise to domain-specific morphology. To this end, we identified the target genes of HOXA11 and HOXA13 in the limb bud by ChIP-Seq analysis. We found that they share common target sequences that contain multiple evolutionarily conserved HOX binding sites and the representative target sequences possess limb-bud specific enhancer functions. We also found that common target genes expressed in the mesenchyme and developing cartilage exhibited differential control by HOXA11 and HOXA13 that may explain the unique autopodal cartilage developmental program.

2 | MATERIALS AND METHODS

2.1 | Animal experimentation

This study was approved by the Institutional Animal Care and Use Committee of the Graduate School of Science and carried out according to the Nagoya University Animal Experimentation Regulations. The *Hoxa13* targeted mice (Fromental-Ramain et al., 1996) were obtained from Dr. Pierre Chambon. The $HoxD^{del(11-13)}$ allele (Zakany, Fromental-Ramain, Warot, & Duboule, 1997) and the *Ulnaless* (Peichel et al., 1997) were provided by Dr. Denis Duboule. Noon on the day the vaginal plug was observed was considered as E0.5. The embryos were isolated by cesarean incision and genotype was assessed by PCR.

2.2 | Chromatin immunoprecipitation (ChIP)

Production of the anti-HOXA13 antibody was described previously (Yokouchi et al., 1995). The method for production and purification of the anti-HOXA11 antibody was also previously described (Yamamoto et al., 1998). The antibodies used in the present study were prepared from rabbits. ChIP was performed according to a standard protocol

(Green & Sambrook, 2012) with the following modifications. Whole limb buds from E11.5 and the autopod from E11.0 wild-type ICR mice were dissected in ice-cold PBS. Embryonic tissues were homogenized 13 times with a tight-fitting Dounce homogenizer, then fixed in 1% formaldehyde/PBS for 10 min at 4°C and quenched with 0.1 M glycine. The cross-linked material was sonicated to produce 200–1,000 bp fragments with a DNA Shearing System S2 (Covaris). The immunoprecipitations were performed with 11 pairs of autopods from E11.0 embryos or 12–18 pairs of whole limb buds from E11.5 embryos. Pierce™ Protein A/G magnetic beads (Thermo Scientific) were conjugated with 10 μg of anti-HOXA13 (Yokouchi et al., 1995) or 8 μg of anti-HOXA11. Sonicated chromatin was incubated with the antibody-protein A/G beads complex overnight at 4°C with rotation. ChIP DNA fragments and control input DNA fragments were converted to a sequence library by NEB Next Ultra™ DNA Library Prep kit for Illumina (NEB) then analyzed by using a HiSEQ 1500 (Illumina). E12.5 ChIP-Seq was performed as described previously (Beccari et al., 2016). For data analysis of E12.5 ChIP-Seq, distal ChIP data and proximal ChIP data were combined. HOXA13 ChIP sequence data were analyzed by Bowtie 2.2.2 (Langmead & Salzberg, 2012) and MACS 2.1.0 (Zhang et al., 2008) (mm9) organized by SraTailor (Oki et al. 2014) under default parameters except 2.15e09 was used for the mouse genome size. For the analysis of HOXA11 ChIP-Seq by MACS2.1.0 (mm9), the following parameters were used: –nomodel, –extsize 200, -g 2.15e09. NGS sequence data of input DNA without ChIP were used as the reference. Overlapping of the ChIP peaks was determined by Bed Tools/ Intersect intervals (Quinlan & Hall, 2010) via Galaxy (Giardine et al., 2005). ComputeMatrix/NGS: DeepTools and plotHeatmap/NGS: DeepTools (Ramirez et al., 2016) in Galaxy were used for creating the aggregate plot. To analyze the sequence conservation around the HOX ChIP summit, the bed file in mm9 format was first converted to mm10 format using the LiftOver tool of the USCE genome browser (Karolchik et al., 2004) then analyzed with the same method used to prepare the aggregate plot using mm10.60way. phastCons.bw data obtained from the UCSC genome browser. For the analysis of sequence motif enrichment, the genomic spans given in BED format were first converted to FASTA files using UCSC Table Browser then analyzed by MIME-ChIP (Machanick & Bailey, 2011). ChIP-Seq data have been deposited in the Gene Expression Omnibus (GEO) with accession number GSE119142.

2.3 | Data analysis

Integrative genome viewer, IGV_2.4.3 (Robinson et al., 2011), was used for graphical analysis of the ChIP-Seq data. Data analysis was also performed using the online application provided by CEAS (Shin, Liu, Manrai, & Liu, 2009) for positioning the ChIP DNA fragments relative to the gene structure, David ver. 6.8 (Huang da, Sherman, & Lempicki, 2009) and Panther ver. 13.1 (Mi, Muruganujan, & Thomas, 2013) for enrichment analysis and classification of the genes, Venny (http://bioinfogp.cnb.csic.es/tools/venny/) for listing common genes in different gene pools, or GREAT (McLean et al., 2010) through the UCSC Genome Browser for identification of the genes neighboring

the ChIP peak using a default parameter. Data sets obtained from the public databases are shown in Supporting Information Table S6.

2.4 | Genechip

Embryos isolated approximately E11.25 were preserved in RNA later (Ambion) and the autopodal tissue corresponding to the *Hoxd13* expressing region was dissected. Total RNA was isolated using the RNeasy Mini Kit (QIAGEN) and biotin labeled RNA was prepared using the IVT Labeling Kit (Affymetrix), One-Cycle cDNA Synthesis Kit (Affymetrix) and Sample Cleanup Modules (Affymetrix). The GeneChip Mouse Genome 430 2.0 Array (Affymetrix) were hybridized, washed, stained and scanned by using standard Affymetrix GeneChip reagents and protocols. Data from two independent experiments were analyzed using the Affymetrix Transcriptome Analysis Console V3.0. Genechip data have been deposited in the GEO with accession number GSE118640. Genes exhibiting more than a 1.5-fold change in the expression ($p < 0.05$) were defined as the HOX13 downstream genes.

2.5 | *In situ* hybridization

Whole-mount *in situ* hybridization (WISH) was performed as previously described (Yamamoto-Shiraishi & Kuroiwa, 2013). Digoxigenin (DIG) or fluorescein-labeled riboprobes were synthesized using the template cDNA fragments amplified with the primer sets listed in Supporting Information Table S5e directly or after cloning into plasmids. Template cDNA clone for the mouse *Hoxd13* probe was provided by Dr. D. Duboule. Generation of the *Bmp2* probe was described previously (Dickinson et al., 1990). Samples were photographed with a Nikon DXM1200F camera system, and the background color was adjusted to obtain best contrast to the signals in each sample. For comparison of the signal patterns between limbs, some limb photographs were flipped horizontally using Adobe Photoshop CS6.

2.6 | Electrophoresis mobility shift assay (EMSA)

The protein coding sequence containing homeobox in the second exon was PCR amplified using the primers presented in Supporting Information Table S5a and connected to the sequence encoding the Maltose binding protein (MBP) in pMal-c (NEB). Protein production and affinity purification were performed according to the manufacturer's instructions (NEB). For preparing the fluorescently labeled probes, aminoaryl labeled double strand DNA was prepared by two-step PCR. The first round of PCR was done using mouse genomic DNA template and RVL-GSP1 and GSP2 primers. This PCR product was then used as the template for the second round of PCR using aminoaryl-RVL and GSP2 as primers. The sequence of each primer is shown in Supporting Information Table S5b. The aminoaryl-labeled DNA fragments were reacted with Alexa Fluor 700 (AF700) NHS ester (Thermo Fisher) in borate buffer then purified using the Qiagen MinElute column (Qiagen). The sequences of the unlabeled competitors are presented

in Supporting Information Table S5c. For the EMSA reaction (25 μl), 0.5 pmoles of AF700 labeled probe was mixed with MBP or MBP-mHOXA11 (or13) HD protein in buffer containing 1 μg poly (dIdC), 20 mM TrisHCl pH 7.5, 150 mM KCl, 0.1% Triton X-100, 1 mM EDTA, 1 mM DTT and 5% glycerol for 30 min at 25°C. After adding 1 μl of 0.05% bromophenolblue solution, the reaction was analyzed by 2% low melting point agarose gel electrophoresis at 4°C using 0.5× TBE as the running buffer. The gel was analyzed with an Odyssey scanner (LI-CORE). For competition experiments, 2.5 pmoles or 25 pmoles of the oligo nucleotides were added to the reaction.

2.7 | Deletion of specific chromosomal regions

Mice with deletion of the putative enhancer of *Tshz2* or *Bmp2* were generated using the CRISPR/Cas9-based genome editing system via electroporation (Hashimoto, Yamashita, & Takemoto, 2016). The guide RNA sequences and deleted regions are presented in Supporting Information Table S5d.

2.8 | Micromass culture and transfection

For micromass culture (MMC), mesenchymal cells of the chicken distal limb bud were prepared as previously described (Yamamoto-Shiraishi, Higuchi, Yamamoto, Hirano, & Kuroiwa, 2014), except Dispase I (WAKO) was used instead of trypsin (final concentration of dispase: 2,000 U/ml). For transfection of MMC, 0.9 μl FuGENE HD (Promega) was mixed with 4.4 μl F-12 and 300 ng plasmid DNA (containing 100 ng pCAGGS-*H2B-EGFP*, and 200 ng pCAGGS, pCAGGS-mouse *Bcl11a*, or pCAGGS-mouse *Bcl11b*, respectively). After incubation for 20 min, 13.2 μl cell suspension (2.5×10^7 cells/ml) containing 2% FBS was added, and cells were seeded onto a glass base dish (ø = 3.5 cm). After incubation in 5% CO_2 at 37°C for 2 hr, 10% FBS/F-12 was added (1 ml/dish). Medium was changed every day. After the incubation for 1 or 2 days, MMCs were fixed with 4% PFA/0.1% Tween20/PBS. Anti-Collagen II Ab-2, mouse monoclonal Ab (NeoMarkers, MS-235; dilution: 1/200) and goat anti-mouse IgG (H+L), Alexa Fluor 594 (Thermo Fisher, A-11032; dilution: 1/300) were used as primary and secondary antibodies, respectively. Nuclear staining was performed with DAPI, and MMCs were photographed using a M205FA (Leica) and FV1000 (Olympus). Col II immuno-fluorescence signal intensity around each nucleus was calculated using Image J. cDNA fragments encoding the mouse *Bcl11a* and *Bcl11b* protein coding sequence were amplified from reverse transcripts of E11.5 limb bud RNA using primer sets presented in Supporting Information Table S5f and were cloned into the pCAGGS vector.

3 | RESULTS

3.1 | *Hoxa11* and *Hoxa13* have distinctive expression domains in the limb bud

Hoxa11 and *Hoxa13* show unique expression pattern along the proximodistal axis in the mesenchyme of the E11.75 mouse forelimb bud

(Figure 1a,b). At this stage of limb development, formation of the zeugopodal cartilage anlage is complete and the carpal and metacarpal precartilaginous condensations are already visible in a continuous anlage of the autopodal region (Figure 1e). Correlations between the *Hox* expression domain and the cartilage patterning were examined by double staining for the expression of *Hox* and the cartilage marker *Col2a1* (Figure 1c,d). As shown in Figure 1c,f, *Hoxa11* is expressed in the distal zeugopodal region and proximal autopodal region spanning most of the carpal cartilaginous condensation. In contrast, *Hoxa13* is expressed throughout the entire autopodal region (Figure 1d,g). Thus, expression of *Hoxa11* and *Hoxa13* covers different domains along the proximodistal axis and overlaps around their expression
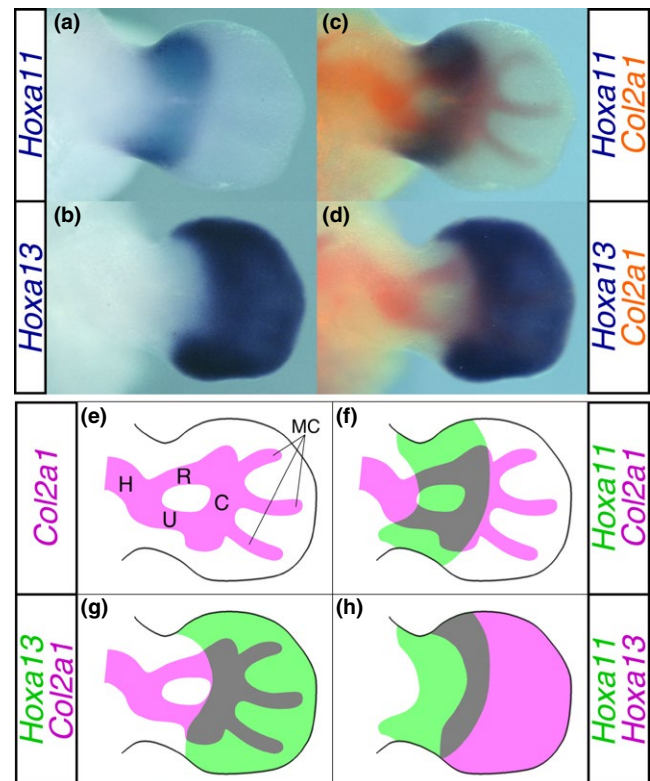

FIGURE 1 Correlation between the *Hox* expression domain and cartilage in the E11.75 mouse forelimb bud. Dorsal view of *in situ* hybridizations for (a) *Hoxa11* and (b) *Hoxa13*. The cartilage pattern was visualized based on the *Col2a1* expression (red) in the same limb bud (c and d). (b) and (d) are presented as a digitally inverted (left-right) views of the original picture. (e) Illustration of the cartilage pattern shown in (c). C: carpus, H: humerus, MC: metacarpus R: radius, U: ulna. (f) and (g) Representative drawings of (c) and (d), respectively. (h) Superimposed view of the *Hoxa11* and *Hoxa13* expression domains. Images redrawn based on relative location of each *Hox* expression domain to the cartilage pattern shown in (f) and (g). The left and right limb buds were isolated from a single embryo at E11.75 and were hybridized with DIG-labeled *Hoxa11* and fluorescein-labeled *Col2a1* probe mixture and DIG-labeled *Hoxa13* and fluorescein-labeled *Col2a1* probe mixture, respectively. *Hox* expression was detected using anti-DIG IgG-alkaline phosphatase (AP) with BM Purple as the substrate (blue). After inactivating AP activity, *Col2a1* expression was detected using anti-fluorescein IgG-AP with Fast Red as the substrate (red)

boundary corresponding to the carpal cartilage anlage (Figure 1h). This same topological correlation between *Hox* expression and cartilage patterning was observed in the E11.75 hindlimb bud (Supporting Information Figure S1A–G).

3.2 | The HOXA11 and HOXA13 DNA binding regions overlap in the limb bud

To assess the zeugopodal and autopodal *Hox* target genes during the cartilage formation at E11.5 when metacarpal/metatarsal anlagen just begins to protrude from carpal/tarsal anlage, we carried out ChIP-Seq analysis and identified the DNA regions associated with HOXA11 or HOXA13 proteins. The number of independent HOXA11 and HOXA13 ChIP peaks was 2,953 and 143,460, respectively (Supporting Information Table S1a). The number of HOXA11 peak is comparable to that of recently reported HOXC10 ChIP-Seq peak in the E11.5 limb bud (Jain et al., 2018). Figure 2a–c and Supporting Information Figure S2A–C show the integrative genome viewer (IGV) representation of HOXA11, HOXA13 and other homeodomain transcription factor binding sites in the representative gene loci.

In the *HoxA* cluster, HOXA13 binding regions were present in the intron of *Hoxa7* (arrow), the 3′UTR of *Hoxa9* (open arrowhead) and the intron of *Hoxa11* (arrowhead) (Figure 2a). The *Hoxa11* intronic binding site is crucial for HOXA13-dependent repression of *Hoxa11* in the autopod (Kherdjemil et al., 2016). In contrast to the binding of both HOXA11 and HOXA13 to the *Hoxa7* and *Hoxa9* regions, only HOXA13 binding was observed in the *Hoxa11* intron. This indicates different contributions of HOXA11 and HOXA13 to the control of *Hoxa11* expression.

As shown in the IGV for other representative gene loci (Figure 2b,c and Supporting Information Figure S2A–C), multiple HOX11/13 binding sites are present and many of the HOXA11 and HOXA13 binding sites overlap with each other. To further analyze this overlap, we determined the accumulation of ChIP-Seq reads around the peak summit. As shown in Figure 3a, significant accumulation of the HOXA13 ChIP-Seq signal was found within 200 bp of the HOXA11 ChIP peak and *vice versa* (Figure 3b). We selected regions that showed the summit of each peak located within 1 kb. Of these colocalized sites, 75% of the ChIP-peak summits were located within 200 bp of each other (Figure 3c). The results that the summits are in close proximity and that both HOXA11 and HOXA13 bind the same target sequence *in vitro* (Shen, Rozenfeld, Lawrence, & Largman, 1997), suggest that they bind the same target *in vivo*. We further selected regions that exhibited directly overlapping peak spans and found that 2,139 HOXA11 binding regions of their expression domain (distal zeugopod and proximal autopod) overlapped with the autopodal HOXA13 peak. These overlapping peaks are 72% of the total HOXA11 peak (Supporting Information Table S1a) indicating that a considerable portion of the HOXA11 binding regions is common to the HOXA13 binding region. We subsequently refer to this common region as the CHBRL (Common Hox binding region of the limb bud). Significant accumulation of both

HOXA11 and HOXA13 ChIP-Seq reads was confirmed around the CHBRL (Figure 3d).

As shown in Figure 3e, the CHBRL was located a long distance (50–500 kb) from the transcription start site (TSS) and most of the CHBRL was located within the intronic or intergenic region (Figure 3f). We also analyzed HOXA13 binding in the E11.0 and E12.5 limb bud and found a considerable portion of the CHBRL (E11.5) was common to both E11.0 (798/2,139, 37%) and E12.5 (1,618/2,139, 76%) HOXA13 ChIP peaks (Supporting Information Table S1b).

3.3 | The CHBRL overlaps with limb SHOX2, PBX, GLI3 or PITX1 binding regions

The homeodomain transcription factors SHOX2 and PBX are also expressed in the limb bud mesenchyme and have important roles in limb cartilage development (Cobb, Dierich, Huss-Garcia, & Duboule, 2006; Selleri et al., 2001). In addition, as shown in Figure 2a–c and Supporting Information Figure S2A–C, some HOX binding regions displayed overlap with the SHOX2 and/or PBX binding peaks suggesting that they may share common targets with HOX11/13. We thus analyzed the overlap between the HOX11/13 binding region and the reported SHOX2, or PBX binding region (Ye et al., 2016). Reported ChIP-Seq reads for both SHOX2 and PBX significantly accumulated around the CHBRL (Figure 3g). As shown in Figure 3j,k, Supporting Information Table S1b, and Supporting Information Figure S2, a substantial number of the HOX11/13 binding regions overlapped with the SHOX2 and/or PBX binding regions, although they exhibited variation in their combinations. The HOX11/13 binding region of *Bmp2* (Figure 2b), *Tshz2*, *Jag1* and *Shox2* (Supporting Information Figure S2A–C, respectively) overlapped with the SHOX2 binding regions; however, the major HOX11/13 binding region in the *HoxA* cluster did not show overlap with SHOX2 binding (Figure 2a). In contrast, some of the HOX11/13 binding regions in *Aff3* overlapped with the SHOX2 binding regions, although other HOX11/13 binding regions in *Aff3* did not show SHOX2 binding (Figure 2c). HOX and SHOX2 share a common binding core sequence *in vitro* suggesting they may also share common binding sites *in vivo* or they bind to different sites in the CHBRLs, as multiple HOX11/13 binding sites are demonstrated in Figure 4. On the other hand, our results also indicate variation in the overall binding repertoire of each homeodomain transcription factor.

The transcription factor GLI3 also has a crucial role in limb morphogenesis as the target of the *Shh* signaling pathway (Buscher, Bosse, Heymer, & Ruther, 1997). Because GLI3 cooperates with 5′ *Hox* genes in cartilage pattern formation of the limb (Chen et al., 2004; Zakany, Zacchetti, & Duboule, 2007), we compared the CHBRL with the GLI3 binding regions in the limb bud (Vokes, Ji, Wong, & McMahon, 2008). The ChIP-Seq reads showed modest accumulation around the GLI3 ChIP peak (Figure 3h). Interestingly, 24% (504/2,139; Figure 3l and Supporting Information Table S1b) of the CHBRL overlapped with the GLI3 binding region suggesting
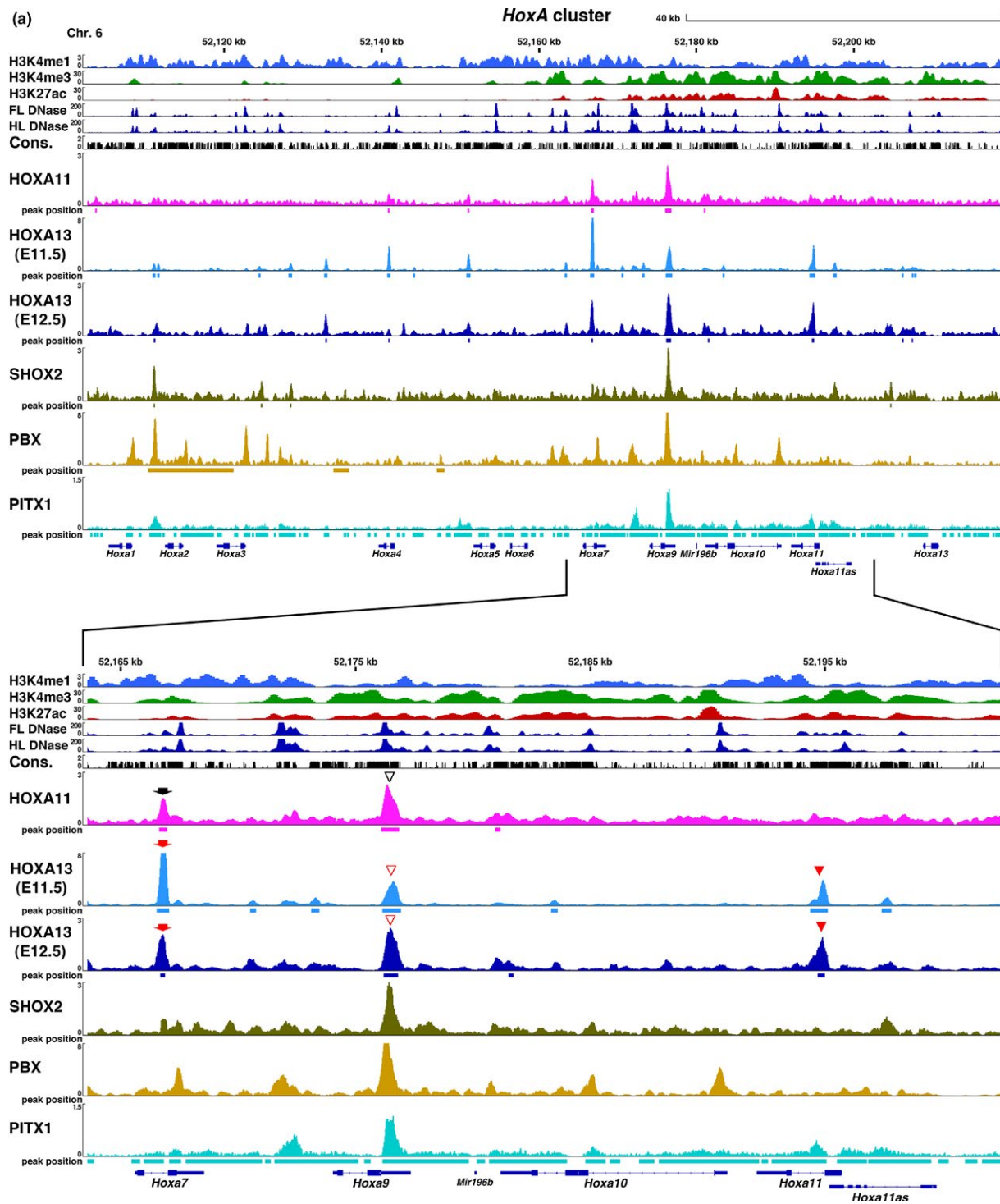
FIGURE 2 IGV view of HOX11/13 and homeodomain transcription factors in the limb bud. (a) *HoxA* cluster, (b) *Bmp2*, (c) *Aff3*. The epigenetic state of each gene determined by enrichment of H3K4me1, H3K4me3 and H3K27ac in the limb buds and DNase I hypersensitivity sites in the E11.5 limb bud (FL DNase, HL DNase, FL: forelimb bud, HL: hindlimb bud) and sequence conservation among vertebrates (Phastcons [Vertebrate 30way]) presented as a bar graph. Data were obtained from public data bases as described in Supporting Information Table S6. ChIP-Seq data for HOXA11 and HOXA13 using E11.5 limb bud (HOXA11 and HOXA13(E11.5)) and E12.5 autopod (HOXA13(E12.5)) from this study are presented as a bar graph. The SHOX2 and PBX binding profiles in the E12.5 limb bud and the PITX1 binding profile in the E11.5 hindlimb bud were visualized by reanalysis of published data source presented in Supporting Information Table S6 using the same platform as for the HOX11/13 data. Numbers in the vertical axis indicate coverage values that were scaled by 1,000,000/ total count. Squares beneath the peak indicate the region identified as transcription factor binding by MACS2 analysis. (a) Arrow: intron of *Hoxa7*, open arrowhead: 5′ UTR of *Hoxa9*, arrowhead: intron of *Hoxa11*. (b) Arrow: the CHBRL deleted in *Bmp2cis*KO in Figure 5
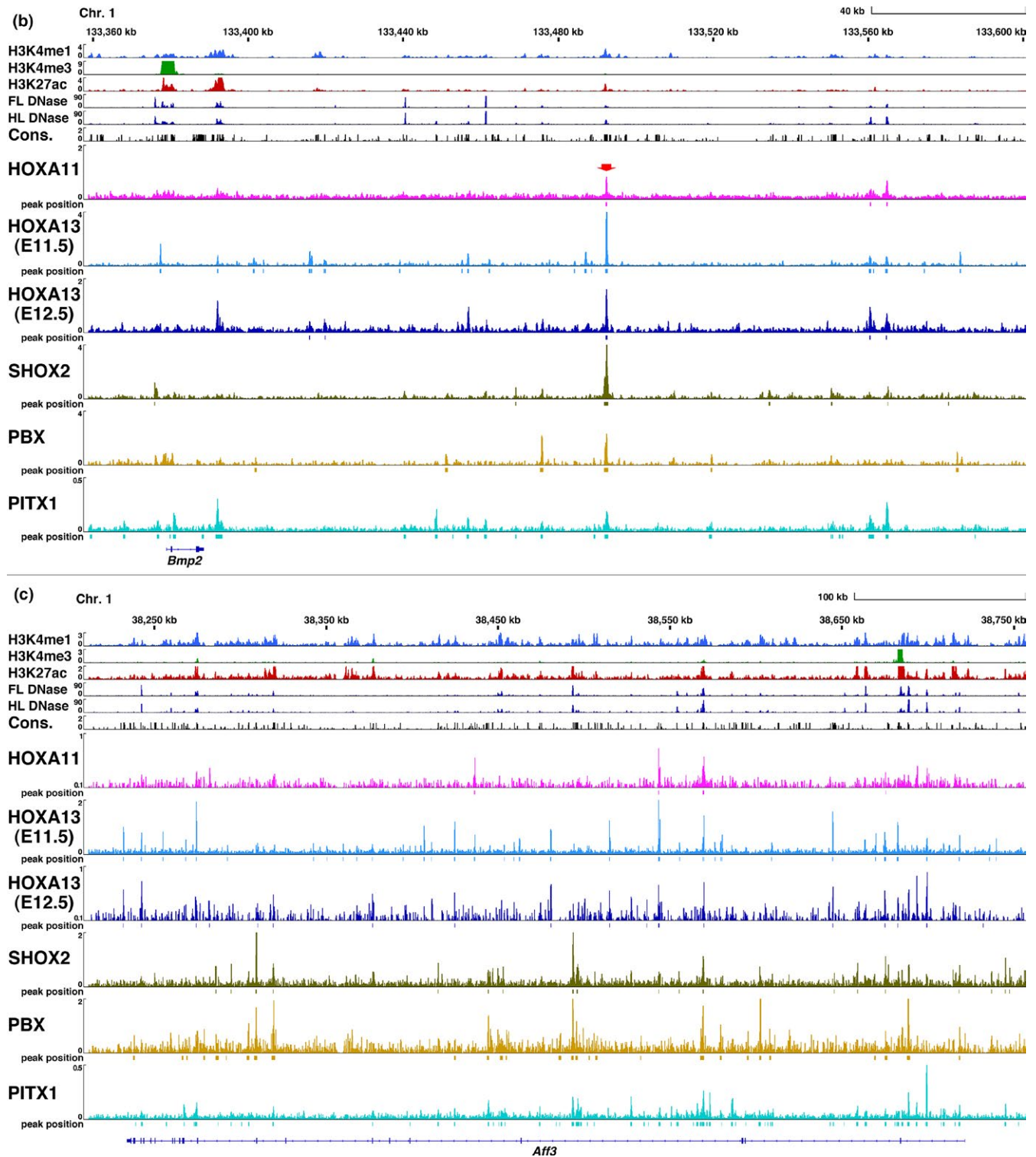
FIGURE 2 Continued

that functional cooperation may occur directly through co-occupation of HOX11/13 and GLI3 in the regulatory element of their target genes (Supporting Information Table S2). The paired-type homeodomain transcription factor PITX1 is also involved in limb cartilage pattern formation (Szeto et al., 1999). As shown in Figure 2a–c, many PITX1 ChIP-Seq peaks overlapped with HOX11/13 peaks and PITX1 ChIP-Seq reads significantly accumulated around the CHBRL (Figure 3i). We found that the 59% of the CHBRL overlapped with the PITX1 binding region (Nemec et al., 2017) (Figure 3m and Supporting Information Table S1b).
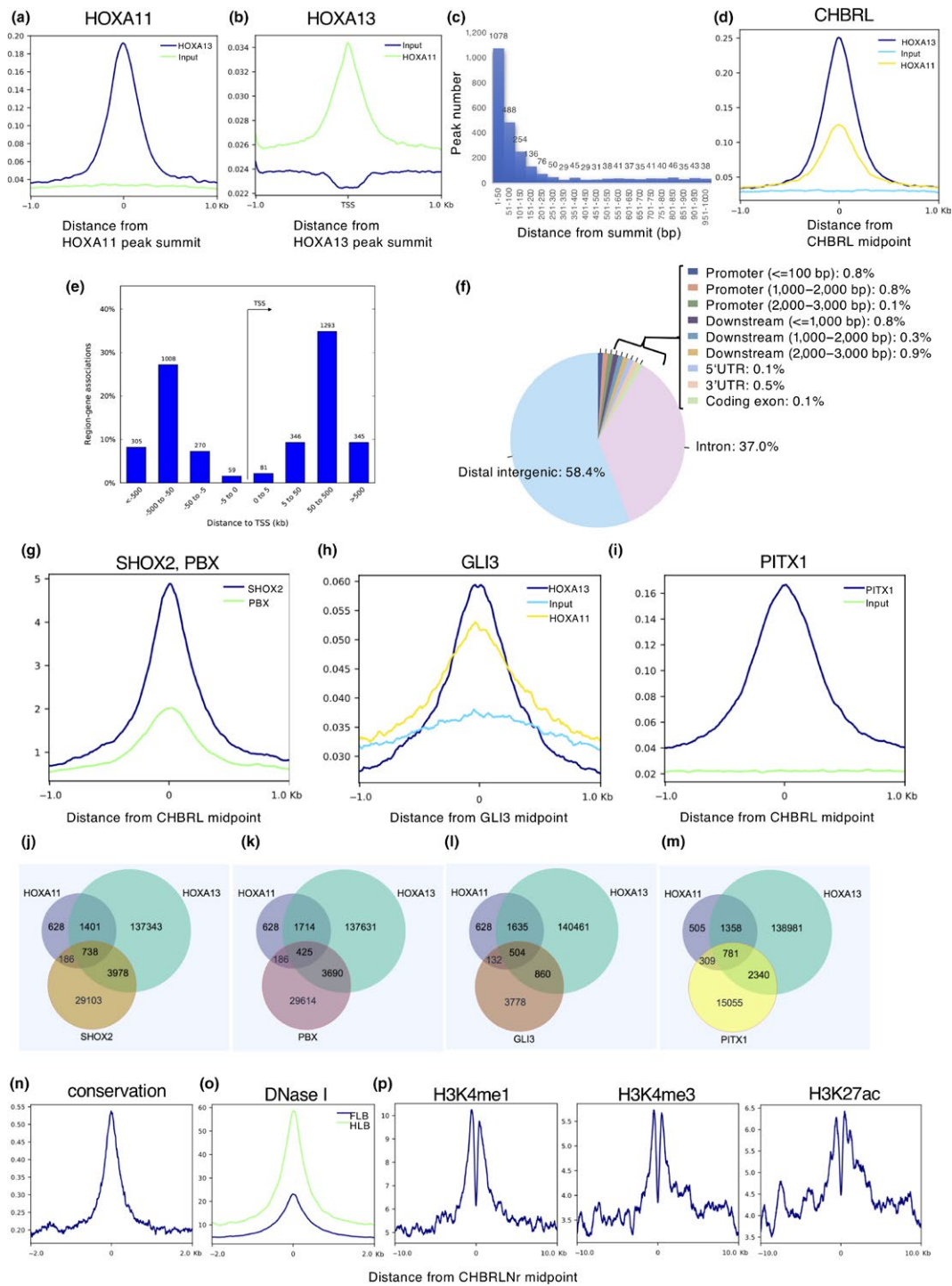
FIGURE 3 Profile of the limb HOX11/13 DNA binding region. Condensed profiles of ChIP-Seq signals of (a) HOXA13 for HOXA11 peak summits or (b) HOXA11 for HOXA13 peak summit. (c) Distribution plot for distances between HOXA11 and HOXA13 peak summits located within 1 kb each other. (d) Condensed profiles of ChIP-Seq signals for the CHBRL. (e) The majority of the CHBRL peaks are located a great distance from their nearest transcription starting site (TSS). (f) The majority of CHBRL peaks are located at the intronic or distal intergenic region of the chromosome. (g) Aggregate plots of SHOX2 and PBX binding signals in the embryonic limb at E11.5 centered around the CHBRL. (h) Aggregate plots of HOXA11and HOXA13 binding signals in the embryonic limb at E11.5 centered around the summits of Gli3 binding region. (i) Aggregate plots of PITX1 binding signals in the embryonic limb at E11.5 around centered around the CHBRL. The number of the overlapping ChIP-Seq peaks of HOXA11 and HOXA13 with (j) SHOX2, (k) PBX, (l) GLI3 and (m) PITX1. (n) Aggregate plots based on average phastcons [60way.phastCons] across vertebrates indicate that the majority of the CHBRLNrs are highly conserved. (o) Aggregate plots on DNase I hyper-sensitive sites in embryonic fore-(FLB) and hindlimb (HLB) at E11.5 around the center of the CHBRLNr. (p) Aggregate plots of H3Kme1, H3K4me3 and H3K27ac binding signals in the embryonic limb at E11.5 around the center of the CHBRLNr. Data source was presented in Supporting Information Table S6. Numbers in the vertical axis of a, b, d, g–i and n–p indicate average signal per base (see Materials and Methods)

3.4 | The CHBRL correlates with limb-specific chromatin epigenetic states

We further analyzed the profile of the CHBRL in relation to the epigenetic state of the limb bud chromatin. After eliminating the regions containing repetitive sequences from the CHBRL pool, most of the remaining regions, the CHBRLNr (CHBRL with no repetitive sequences, 1,518/2,139, 71%; Supporting Information Table S1b) exhibited significant overlap with conserved sequence shared among vertebrates (1,506/1,518, 99%; Figure 3n); a representative comparison is shown in Supporting Information Figures S4 and S5I–L. The DNase I hypersensitive region of the limb bud was significantly localized around the CHBRLNr (Figure 3o). Of the CHBRLNr, 73% (1,107/1,518; Supporting Information Table S1b) showed overlap with the DNase I hypersensitivity region in the E11.5 limb bud (Yue et al., 2014).

To further define the chromatin epigenetic state around the CHBRLNr, we evaluated the histone modification profiles. As shown in Figure 3p, H3K4me1, H3K4me3 and H3K27ac were enriched around the CHBRL. Representative overlapping of the HOXA11 or HOXA13 peaks with the modified histone region is also shown in Figure 2a–c and Supporting Information Figure S2A–C. Interestingly, 70% (1,063/1,518; Supporting Information Table S1b) of the conserved CHBRLNr overlapped with the region enriched for H3K27ac suggesting that a significant part of the CHBRLNr participates in potential enhancer function in the limb bud. A deep trough in the middle of the histone modification peaks shown in Figure 3p suggests that CHBRLNr corresponds to a nucleosome-free (depleted) region. This is supported by the fact that DNase I hyper-sensitive sites are enriched around CHBRLNr shown Figure 3o. By matching with the limb enhancer regions provided by the VISTA program (Visel, Minovitsky, Dubchak, & Pennacchio, 2007), 57 regions out of 334 regions in the VISTA limb enhancer were found to correspond with the CHBRLNr (Supporting Information Table S1b) including the *Shox2* enhancer (Osterwalder et al., 2018; Rosin, Abassah-Oppong, & Cobb, 2013) located in the intron of the neighboring gene *Rsrc1* (Supporting Information Figure S2C arrow). In addition, the CHBRLNr shown in Figure 2b (arrow) was also included in the region possessing the distal limb bud enhancer of *Bmp2* (Dathe et al., 2009). These results indicate that a particular member of the CHBRLNr actually possesses the limb-specific enhancer function.

3.5 | Multiple HBSs were enriched in the HOX11/13 ChIP fragments

ABD-B type HOX proteins bind to both the TTAT/C and TAAT/C motifs (HOX binding sequence: HBS) *in vitro* (Shen et al., 1997). We thus analyzed the enrichment of these sequences in the HOXA11 and HOXA13 ChIP fragment and the CHBRLNr. As shown in Supporting Information Figure S3, the sequences containing TTAT or TAAT were highly enriched in the HOX11/13 ChIP fragment indicating that HOX11/13 proteins directly bind to the majority of the ChIP fragment *in vivo*. Interestingly, as shown in representative results in Supporting Information Figures S4B,C and S5I–L, evolutionarily conserved multiple HBSs were found in most of the ChIP DNA.

3.6 | HOX11/13 protein directly binds to the evolutionarily conserved HBSs in the ChIP DNA

As described above, the nucleotide sequences encoded by most HOX11/13 ChIP fragments showed evolutionary conservation. Among them, the HOX protein binding consensus core sequence, HBS, exhibited a high level of conservation (Supporting Information Figures S4B,C and S5I–L). We then analyzed direct HOX11/13 protein binding to typical CHBRLs *in vitro* by EMSA.

One of the CHBRLs in the *Rsrc1* intron (Supporting Information Figure S2C, arrow), m741 (VISTA), carries the limb-mesenchyme specific enhancer function of the neighboring *Shox2* gene (Osterwalder et al., 2018; Rosin et al., 2013). m741 contains highly conserved multiple HBSs, which are concentrated in the two sub-regions, 741b and 741c (Supporting Information Figure S4). As shown in Figure 4a,b and Supporting Information Figure S5a,b, in the presence of HOXA13HOMEODOMAIN (HD) both the 741b and 741c probes showed multiple shift bands in a HOXA13HD protein dose-dependent manner indicating that HOXA13 has multiple binding sites in the probe. These shift bands were competed by oligonucleotides containing HBS1 (TTAT) or HBS2 (TAAT) but not competed by oligonucleotides containing mutated HBS (Figure 4b and Supporting Information Figure S5B). HOXA11HD also showed the same binding profile as HOXA13HD to the 741b and 741c probes (Figure 4c,d and Supporting Information Figure S5C,D). These results indicate that HOX11/13 protein directly binds to the HBSs in the 741b and 741c. The CHBRLs of *Bmp2*, *Jag1* and *Tshz2*, in addition to one of the *Aff3* CHBRLs, also contain multiple

FIGURE 4 HOXA11 and HOXA13 bind to multiple HBSs in the CHBRL *in vitro*. EMSAs using 741b, a part of the *Shox2* CHBRL/m741 enhancer (VISTA), as a probe. (a) Multiple shift bands emerged in a HOX protein dose-responsive manner; (–): no protein; MBP: 153 ng of MBP was added to the reaction. The amount of MBP-HOXA13HD used was 7.6, 15.2, 42, 85, 152, 152, 306 and 612 ng. (b) Band shift was competed by HBS-containing oligonucleotides HBS1 (TTAT) and HBS2 (TAAT) but not by their mutant forms (T to G and A to C). 153 ng of MBP and 128 or 255 ng of MBP-HOXA13HD were used. 5-fold or 50-fold excess molar unlabeled competitor was added to the reaction. (c) Multiple shift bands emerged in a HOX11/13 protein dose-responsive manner; (–): no protein, MBP; 153 ng of MBP was added to the reaction. The amount of MBP-HOXA11HD added was 1.4, 2.8, 5.7, 11.4, 28, 57, 57, 114, 228 ng. (d) Band shift was competed by HBS containing oligonucleotides HBS1 (TTAT) and HBS2 (TAAT) but not by their mutant forms (T to G and A to C). 153 ng of MBP and 95 or 189 ng of MBP-HOXA11HD were used. 5-fold or 50-fold molar excess unlabeled competitor was added to the reaction. (e–h) Multiple shift bands emerged in the HOX11/13 protein in a dose-dependent manner and were specifically competed by HBS-containing oligonucleotides. (e, g) MBP-HOXA13HD and (f, h) MBP-HOXA11HD. (e) and (f) *Aff3* probe, (g) and (h) *Bmp2* probe. The sequence of the probe and conserved HBS are shown in Supporting Information Figure S5I, J. Arrowhead and arrow indicate the shift band and free probe, respectively. C: competitor, P: protein.
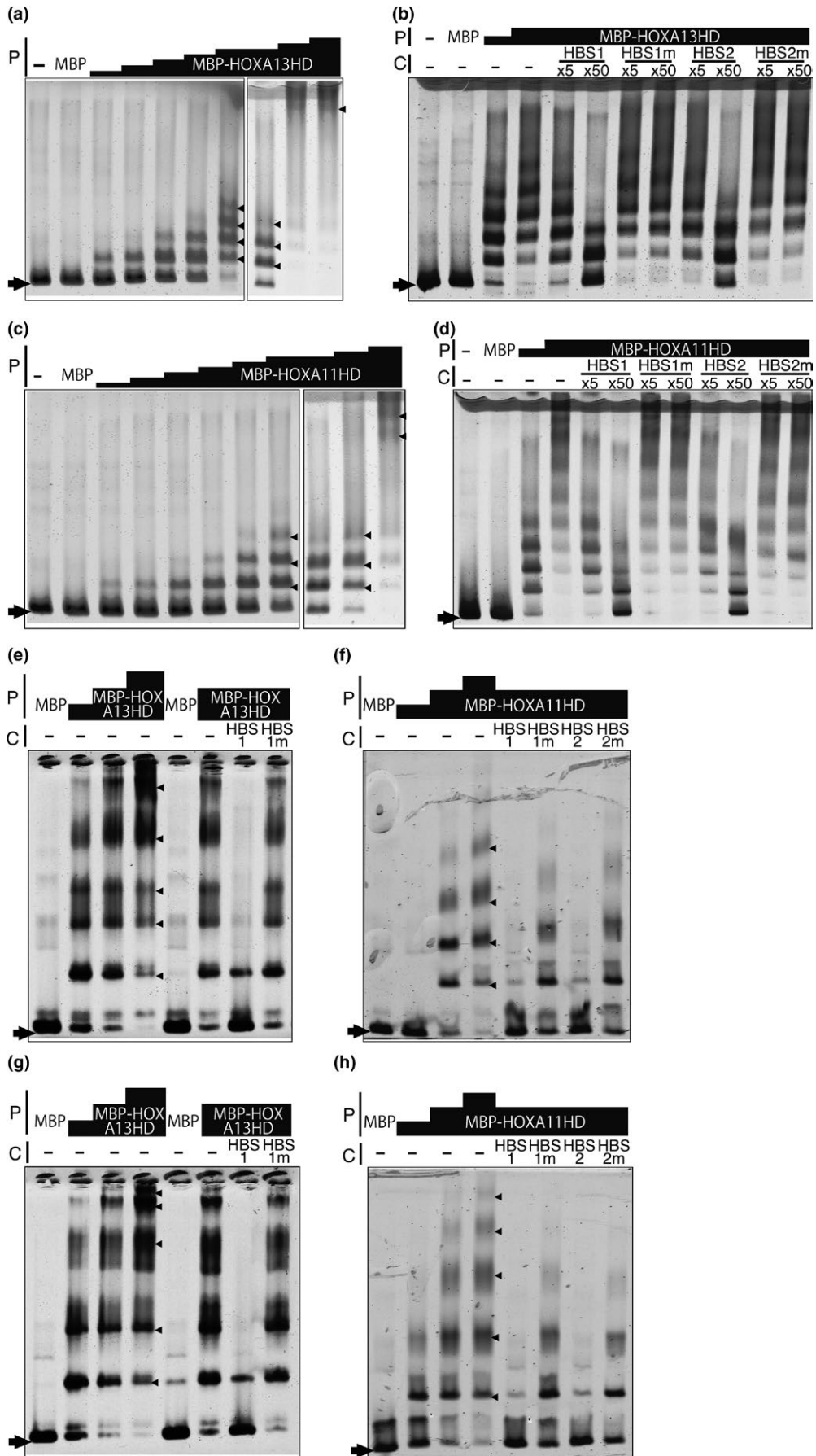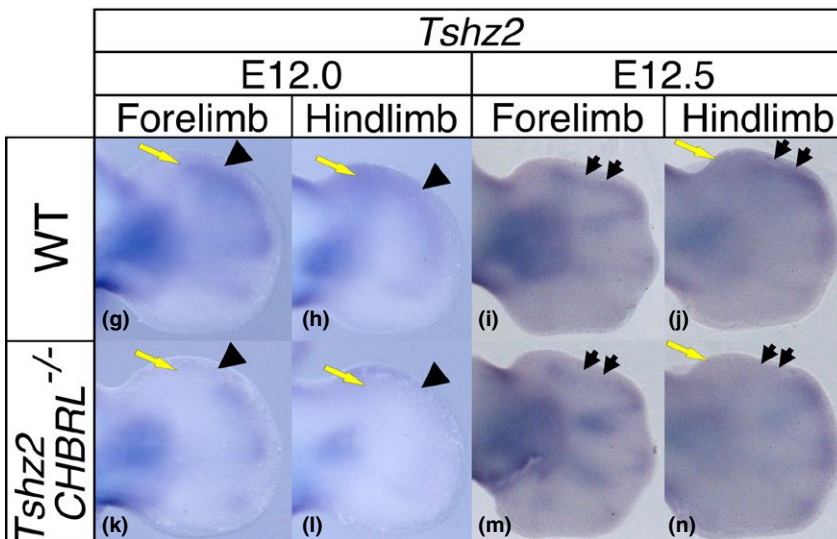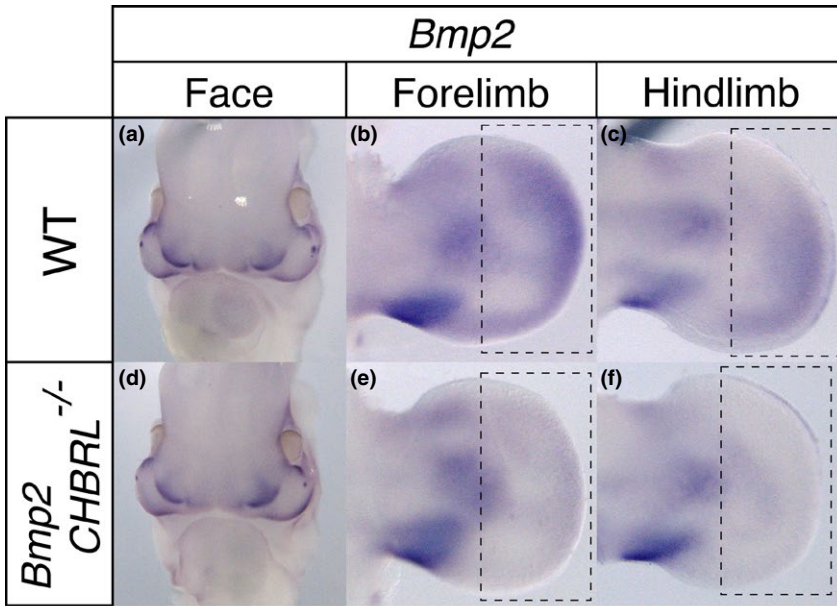
FIGURE 5 CHBRLs of *Bmp2* and *Tshz2* have limb bud-specific enhancer function. Expression pattern of *Bmp2* in (a–c) wild-type and (d–f) *Bmp2CHBRL*^−/− embryos. Facial *Bmp2* expression was not altered in the same (a and d) *Bmp2CHBRL*^−/− embryos. The dotted squares indicate the region exhibiting reduced *Bmp2* expression in *Bmp2CHBRL*^−/− embryos (compare b and e, c and f). Expression pattern of *Tshz2* in (g–j) wild-type and (k–n) *Tshz2CHBRL*^−/− embryos. The arrowhead and arrow indicate the regions exhibiting reduced *Tshz2* expression in *Tshz2CHBRL*^−/− embryos

HBSs (Supporting Information Figure S5I–L). Both HOXA11HD and HOXA13HD bound these fragments in an HBS-dependent manner indicating that HOX11/13 proteins directly bind to the conserved HBSs in the CHBRL (Figure 4e–h and Supporting Information Figure S5E–H).

3.7 | Chromosomal CHBRLs have limb-specific enhancer activity

We next examined if the chromosomal CHBRLs are responsible for regulating neighboring gene expression in the limb bud. Considering that multiple enhancers have redundant function (Osterwalder et al., 2018), we selected *Bmp2* and *Tshz2* as a representative system. Both genes have one or two CHBRLs, so we deleted the most prominent CHBRLs using CRISPR/Cas9 system (*cis*KO). We generated *Bmp2cis*KO mice by deleting 1,623 bp-containing CHBRL located about 100 kb downstream of the *Bmp2* coding region (Figure 2b, arrow) and *Tshz2cis*KO mice by targeting a 1,242 bp chromosomal region in

the intron (Supporting Information Figure S2B, arrow). As shown in Figure 5a–f, in the *Bmp2CHBRL*^−/− embryos, *Bmp2* expression in the distal mesenchyme was considerably reduced in the forelimb bud and barely detectable in the hindlimb bud. In the *Tshz2CHBRL*^−/− embryos, *Tshz2* expression in the first interdigital region was slightly weakened in the forelimb bud and undetectable in the hindlimb bud (Figure 5g–n, arrowheads and black arrows). In addition, weak expression in the anterior autopod was undetectable in both the forelimb and hindlimb buds of the *Tshz2CHBRL*^−/− embryos (Figure 5g,h,j–l,n, yellow arrows). These results indicate that the chromosomal CHBRLs possess the limb mesenchyme enhancer function in the *Hox* expressing domain.

3.8 | Genes neighboring the CHBRLNr show altered expression in *Hox11-13* mutant limbs

We identified 1,556 genes neighboring the CHBRLNr (a11a13 genes, Supporting Information Table S2). Among these, genes

related to skeletal development, limb development or cartilage morphology were enriched (Supporting Information Figure S6A). Interestingly, genes related to skeletal development were also enriched in the gene groups whose CHBRLNr overlapped with the SHOX2, PBX1, PITX1 and GLI3 binding regions (Supporting Information Table S2, Figure S6B–E). We also found that most of the genes containing or neighboring the CHBRLNr belong to the same topologically associating domain (TAD) as the CHBRLNr (1,232/1,556 genes, 79%; Supporting Information Tables S2 and S4) indicating that these CHBRLNrs are involved in regulating the expression of flanking genes (Long, Prescott, & Wysocka, 2016). To verify these as the *Hox* target genes, we analyzed the limb bud expression profile in wild-type and *Hox13* deleted embryos.

Hoxa13 and *Hoxd13* show overlapping expression in the autopodal mesenchyme and cooperatively function in autopodal cartilage pattern formation (Fromental-Ramain et al., 1996; Yokouchi et al., 1991). *Hoxd11* and *Hoxd12* are also expressed in the autopodal mesenchyme and cooperate in autopodal cartilage pattern formation in a gene dosage-dependent manner together with *Hoxa13* and *Hoxd13*. Specifically, homozygote with simultaneous deletion of *Hoxd11,12,13* (*HoxD*$^{del(11-13)}$) exhibited more severe adult cartilage phenotypes than *Hoxd13* KO homozygotes (Zakany et al., 1997). To increase the sensitivity in analyzing *Hox* function, we combined *HoxD*$^{del(11-13)}$ and *Hoxa13*KO mice in this study (we abbreviate *Hoxa13*$^{-/-}$; *HoxD*$^{del(11-13)/del(11-13)}$ as *Hox13*dKO).

We isolated RNA from the autopod of wild-type and *Hox13*dKO embryos and quantified the transcript levels by Genechip (Supporting Information Table S3a,b). To minimize overrepresentation of the genes related to cartilage differentiation caused by loss of the *Hox13* function (Supporting Information Figure S7) and to concentrate early responding genes to the loss of *Hox13* function, we isolated tissue from E11.25 embryos where only the carpal/tarsal anlage had developed in the autopodal region. In addition, to avoid the effect of stylopod and zeugopod gene expression on changes in their expression in the *Hox13*dKO autopod, we isolated the distal autopodal tissue that roughly corresponded to the *Hoxd13* expressing region.

Of the 781 genes showing upregulation in the E11.25 mutant autopod, 102 genes were included among the CHBRLNr genes (Supporting Information Table S2 and Figure S8A). Interestingly, genes categorized under "transcription regulation" were enriched in this cluster (*p* = 1.16E-19, 41/102, Supporting Information Table S3c and Figure S8B). Among the 805 genes showing downregulation in the *Hox13*dKO autopod, 79 genes overlapped with the CHBRLNr genes (Supporting Information Table S2 and Figure S8A) exhibiting their functional variability (Supporting Information Figure S8C). Interestingly, three genes belong to both classes due to their alternate exon usage. Following these analyses, we referred to any CHBRLNr genes showing alteration in the *Hox13*dKO as direct *Hox* target genes. It is curious that many of the genes exhibiting expression changes in the mutant autopod were not included in the CHBRLNr genes. Given that a number of transcription factor-coding genes are HOX13 target, the genes not included in CHBRLNr gene group are likely to be the downstream of *Hox* target transcription factors.
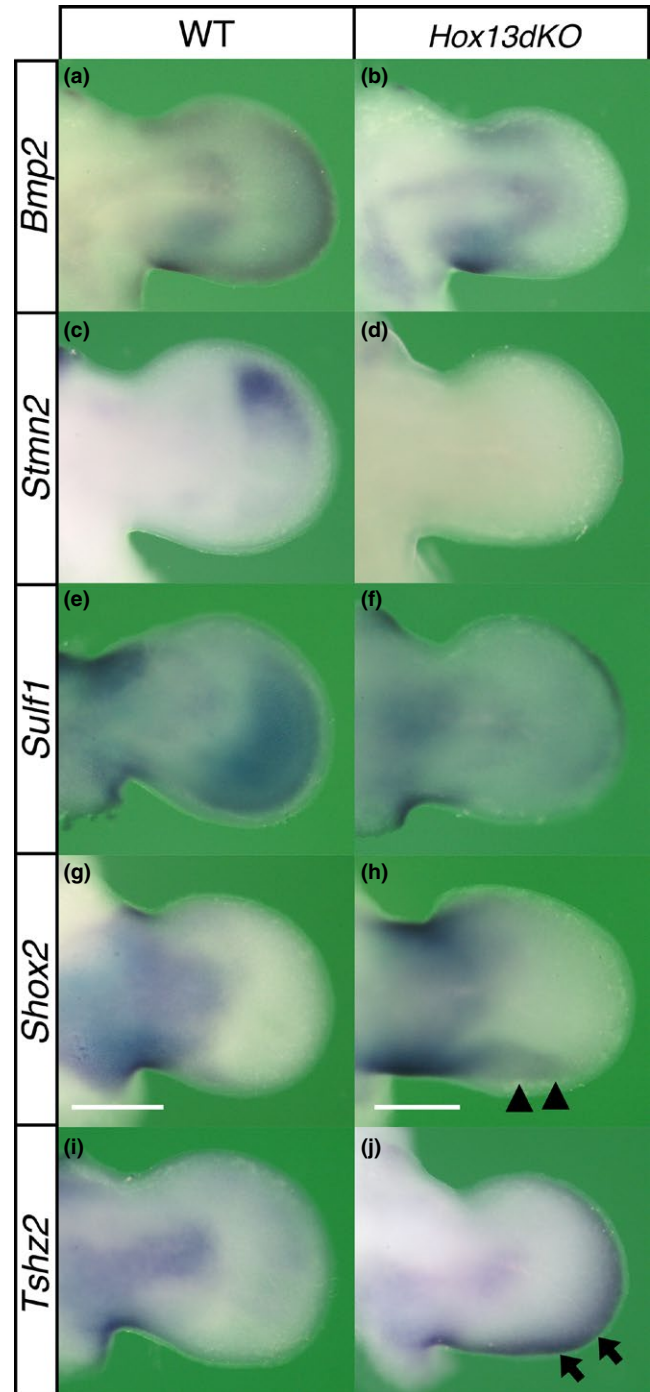

FIGURE 6 Altered gene expression patterns in the *Hox13*dKO autopod. Dorsal view of gene expression detected by *in situ* hybridization in E11.25–11.5 (a, c, e, g, i) wild-type and (b, d, f, h, j) *Hox13*dKO forelimb buds. The expression of (a and b) *Bmp2*, (c and d) *Stmn2* and (e and f) *Sulf1* in the autopodal mesenchyme was reduced or undetectable in the *Hox13*dKO embryos. In contrast, (g and h) *Shox2* and (i and j) *Tshz2* showed ectopic expression in the *Hox13*dKO autopod. Since *Hoxa13* KO mice were generated by inserting *Neo* sequence in *Hoxa13* locus, *Neo* expression mimics *Hoxa13* expression. In order to define the autopod as the region expressing *Hoxa13* in the *Hox13*dKO mice, contralateral limb bud of each specimen was hybridized with *Neo* probe (results not shown). Scale bar indicates 500 μm

3.9 | Changes in the spatial expression pattern of HOX11/13 target genes in the *Hox11-13* mutant limb bud

We next analyzed the changes in the spatial expression pattern of HOX11/13 target genes in loss-of-function *Hox13* mutant limb

buds. In *Hox13*dKO embryos, the cartilage pattern in the limb at E11.25 showed no obvious changes; however, at E12.5 the interdigital region was missing and a single flat cartilage was present instead of the five metacarpi and phalanges (Supporting Information Figure S7) indicating disorganized patterning of the autopodal cartilage. As representative genes exhibiting altered
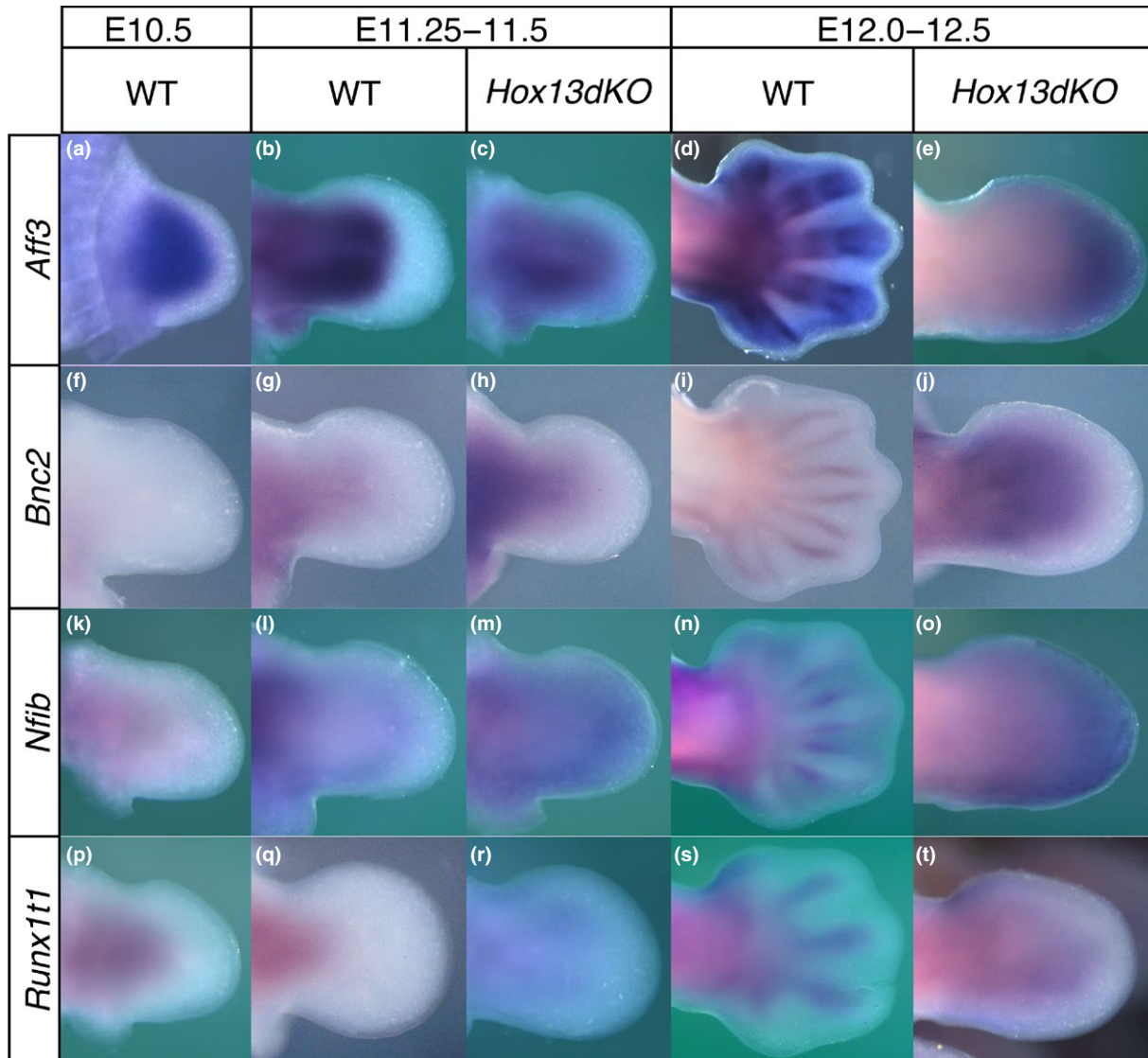

FIGURE 7 Transition in the spatial expression pattern of the genes encoding *Hox* target transcription factors associated with cartilage differentiation and changes in the *Hox13*dKO autopod. Dorsal view of gene expression detected by *in situ* hybridization in the forelimb bud at (a, f, k, p) approximately E10.5, (b, c, g, h, l, m, q, r) E11.5 and (d, e, i, j, n, o, s, t) E12.5. (a) In wild-type embryos, *Aff3* was expressed throughout the entire limb bud mesenchyme excluding the narrow distal most region at E10.5. *Aff3* expression was not found in the autopod at (b) E11.5; however, at (d) E12.5 expression was detected in the cells in/around the perichondrium of the autopod but not in the interdigital mesenchyme. In *Hox13*dKO embryos, *Aff3* expression expanded to the proximal autopodal region (c) at E11.5 then the expression was observed throughout the entire autopodal mesenchyme (e) at E12.5. *Bnc2* expression was not detected in the (f) E10.5 mesenchyme but was detected in the center of the stylopod and zeugopod (g) at E11.5. (i) *Bnc2* expression was later found in the perichondrium of the limb cartilage including the autopod at E12.5. *Bnc2* expression was expanded to the proximal *Hox13*dKO autopod (h) at E11.5 and throughout the entire mesenchyme (j) at E12.5. *Nfib* expression was found in the proximal region of the (k) E10.5 limb bud then in the zeugopod/autopod boundary region at (l) E11.5. (n) *Nfib* expression was detected in the perichondrium of the autopodal cartilage at E12.5. In the *Hox13*dKO limb bud, expression was detected throughout the entire autopodal mesenchyme both (m) at E11.5 and (o) E12.5. *Runx1t1* expression was detected in the proximal center of the (p) E10.5 and (q) E11.5 limb but excluded from the autopodal region. (s) In the E12.5 autopod, *Runx1t1* expression was detected in the cartilaginous condensation. In *Hox13*dKO embryos, *Runx1t1* expression was expanded to the proximal autopod at (r) E11.5 and the central region of the autopod showed expression at (t) E12.5

expression in the *Hox13*dKO limb, we first chose *Bmp2*, *Sulf1* and *Stmn2* as downregulated genes, and *Aff3*, *Shox2* and *Tshz2* as up-regulated genes in the *Hox13*dKO limb. These genes are also common targets of HOXA11, HOXA13, SHOX2, PBX and PITX1 in the limb bud.

Bmp2 was expressed in the mesenchyme of the distal autopod in the wild-type limb and while the expression was not altered in the *Hoxa13*$^{+/-}$ and *Hoxa13*$^{-/-}$ limb, it was reduced in the *HoxD*$^{del(11-13)/del(11-13)}$ and undetectable in the *Hox13*dKO limb bud (Figure 6a,b and Supporting Information Figure S9A). *Stmn2* was expressed in the mesenchyme of the anterior autopod of E11.5 wild-type and *Hoxa13*$^{+/-}$ forelimb buds. The intensity of the autopodal expression signal was not affected in the *Hoxa13*$^{-/-}$, although it was expanded posteriorly in the *HoxD*$^{del(11-13)/del(11-13)}$ limb bud. In the *Hox13*dKO limb bud, *Stmn2* expression was undetectable in the autopod (Figure 6c,d and Supporting Information Figure S9B).

Sulf1 was expressed in the autopodal mesenchyme of E11.5 wild-type and *Hoxa13*$^{+/-}$ forelimbs. The intensity and area of autopodal expression were decreased in both *Hoxa13*$^{-/-}$ and *HoxD*$^{del(11-13)/del(11-13)}$ limbs. The expression signal was further reduced or undetectable in the *Hox13*dKO autopod (Figure 6e,f and Supporting Information Figure S9C). *Sulf1* showed dynamic change in the AER expression (Lewandowski et al., 2015) and this expression was affected indirectly by *Hox11-13* mutation (Figure 6e,f and Supporting Information Figure S9C, see detail in Supporting Information Figure S9 legend).

Aff3, encoding an AF/FMR2 family transcription factor, was expressed in the E11.5 wild-type zeugopod but not in the autopod. In the E11.5 *Hoxa13*$^{-/-}$ limb, *Aff3* expression was expanded into the autopod and *Aff3* expression was detected in the entire autopodal region of the *Hox13*dKO limb (Figure 7b,c and Supporting Information Figure S9D, see detail in Supporting Information Figure S9 legend).

Shox2 was expressed in the E11.5 wild-type zeugopod but undetectable in the autopod, and the expression was not affected in E11.5 *HoxD*$^{del(11-13)/del(11-13)}$ and *Hoxa13*$^{-/-}$ mice (Supporting Information Figure S9E). In contrast, in the E11.5 *Hox13*dKO mice, *Shox2* expression was expanded into the posterior autopodal region (Figure 6g,h, arrowhead).

Tshz2 is expressed in the E11.5 zeugopodal mesenchyme but not in the autopod (Caubit et al., 2000). Ectopic *Tshz2* expression was detected in the distal and posterior periphery of the E11.5 *Hox13*dKO autopod (Figure 6i,j, arrow). However, this aberrant expression pattern was not observed in *Hoxa13*$^{-/-}$ or *HoxD*$^{del(11-13)/del(11-13)}$ mice (Supporting Information Figure S9F). Thus, genes that exhibited altered expression levels in the *Hox13*dKO autopod in Genechip analysis actually showed unique changes in the spatial expression pattern in the *Hox13*dKO limb bud.

We further analyzed the expression of the *Hox13* target transcription factors, *Aff3*, *Bnc2*, *Nfib* and *Runx1t1* whose expression was increased in the *Hox13*dKO autopod. Of these, *Aff3*, *Bnc2* and *Runx1t1* are common target genes of HOXA11, HOXA13, SHOX2, PBX and PITX1 whereas *Nfib* is a common target gene of HOXA11, HOXA13 and PITX1 in the limb bud. *Aff3*, *Bnc2*, *Nfib* and *Runx1t1*

were expressed in the zeugopodal mesenchyme and cartilage but not in the autopod at E11.5 (Figure 7b,g,l,q). Expression of these genes was then also detected in the autopodal cartilage or perichondrium at E12.5 (Figure 7d,i,n,s). In the *Hox13*dKO embryos at E11.5, the expression of *Aff3*, *Bnc2*, *Nfib* and *Runx1t1* were clearly expanded into the autopod (Figure 7c,h,m,r). Thus, representative *Hox* target genes exhibiting increased transcription in the *Hox13*dKO by Genechip were confirmed to be ectopically transcribed in the autopodal mesenchyme in the *Hox13*dKO. The expression of these genes in the zeugopod mesenchyme was already detectable at E10.5 when zeugopodal cartilage formation is just beginning (Figure 7a,k,p) except *Bnc2*. In contrast, expression of these genes was suspended in the autopod mesenchyme at E11.5. Thus, the relationship between the expression of these genes in the mesenchyme and cartilage is different between the zeugopod and autopod.

Thus, a change in the level of a transcripts of a representative gene in the *Hox13*dKO autopod shown by Genechip analysis was verified by WISH analysis.

3.10 | Changes in the *Hox11/13* target gene expression patterns in the *Ulnaless* limb bud

As shown, autopodal expression of a group of the *Hox11/13* target genes such as *Aff3*, *Shox2* and *Tshz2* at E11.5 are probably transiently repressed by *Hox13*. To verify this possibility, we analyzed the effect of *Hoxd13* mis-expression. For this purpose, we adopted *Ulnaless* (*Ul*), which is a dominant mutation of the *HoxD* locus caused by a chromosomal inversion which results in the truncation of both the ulna and fibula due to mis-expression of *Hoxd13* in the posterior zeugopod (Peichel et al., 1997).

In the E11.5 *Ul*/+ mice, *Tshz2* expression in the distal zeugopod was reduced and the expression domain was narrowed at the dorsal zeugopodal region and reduced in the ventral zeugopod (Figure 8a), and *Shox2* expression was weakened at the dorsal posterior and ventral region of the zeugopod (Figure 8b). In the E12.5 *Ul*/+ mice, the *Aff3* signal was undetectable specifically in the ventral zeugopodal region (Figure 8c, arrow). Thus, the expression of these genes in the zeugopod was downregulated in the ectopic *Hoxd13* domain confirming that *Hoxd13* is repressive against the expression of these genes.

3.11 | HOXA13 represses cartilage differentiation of limb mesenchymal cells through BCL11a

Bcl11a encodes a zinc finger-type transcriptional repressor (Liu et al., 2003) whose expression was decreased in the *Hox13*dKO autopod. BCL11a represses blood cell differentiation (Liu et al., 2003), however its function in cartilage differentiation remains elusive.

Bcl11a was expressed throughout the entire limb mesenchyme at E10.5 (Figure 9a), then at E11.5 the expression was detected in the autopodal mesenchyme and the posterior zeugopodal mesenchyme (Figure 9b). At E12.0 the expression was found in the perichondrium of the autopodal cartilage (Figure 9d) where *Hoxa13* was
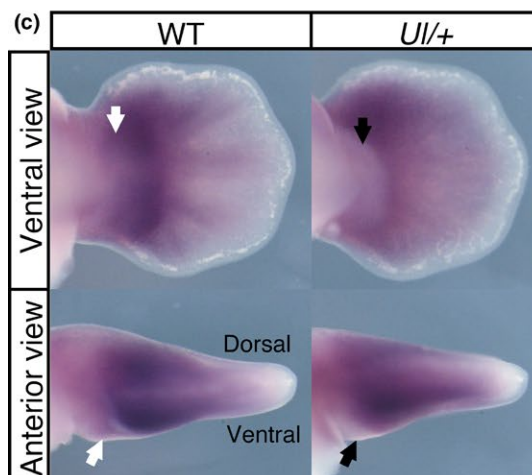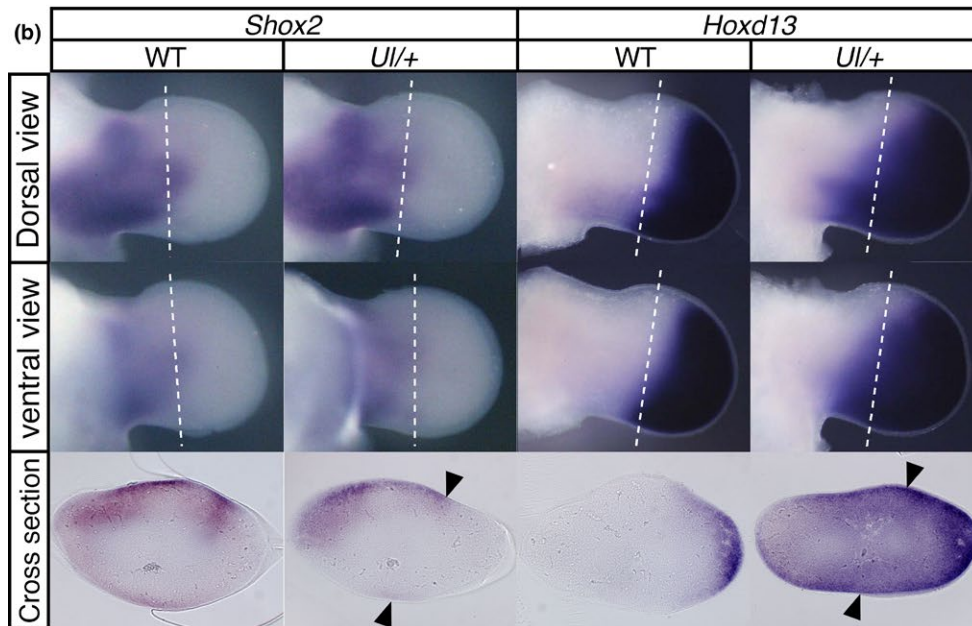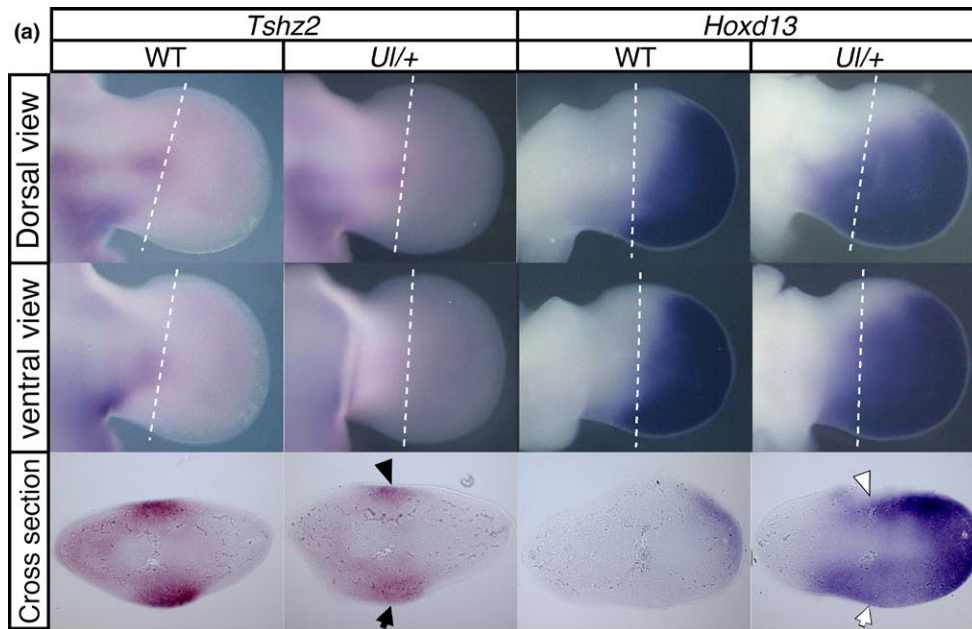
FIGURE 8 In the *Ulnaless* limb, ectopic *Hoxd13* expression represses target gene expression. Expansion of the *Hoxd13* expression domain to more a proximal area overlapping with the zeugopodal region occurred in the *Ul/+* mutant limb. Reduction of (a) *Tshz2*, (b) *Shox2* and (c) *Aff3* expression in the zeugopod region overlapping the ectopic *Hoxd13* expression domain indicates that *Hoxd13* as well as *Hoxa13* represses the expression of these genes. (a) The black arrow and arrowhead indicate the reduced *Tshz2* expression and the white arrow and arrowhead indicate ectopic *Hoxd13* expression. (b) Black arrowheads indicate the tissues with reduced expression of *Shox2* and augmented *Hoxd13* expression. (c) Black arrows indicate the reduction in *Aff3* expression in the *Ul/+* limb and the white arrows indicate the corresponding region in the wild-type limb. Dotted lines in panel a and b indicate the position of cross sections. Ventral views were digitally inverted (left-right). In the panel a and b, the left and right limb buds were isolated from a single embryo at E11.5 and were hybridized with *Tshz2* or *Shox2* probe and *Hoxd13* probe, respectively
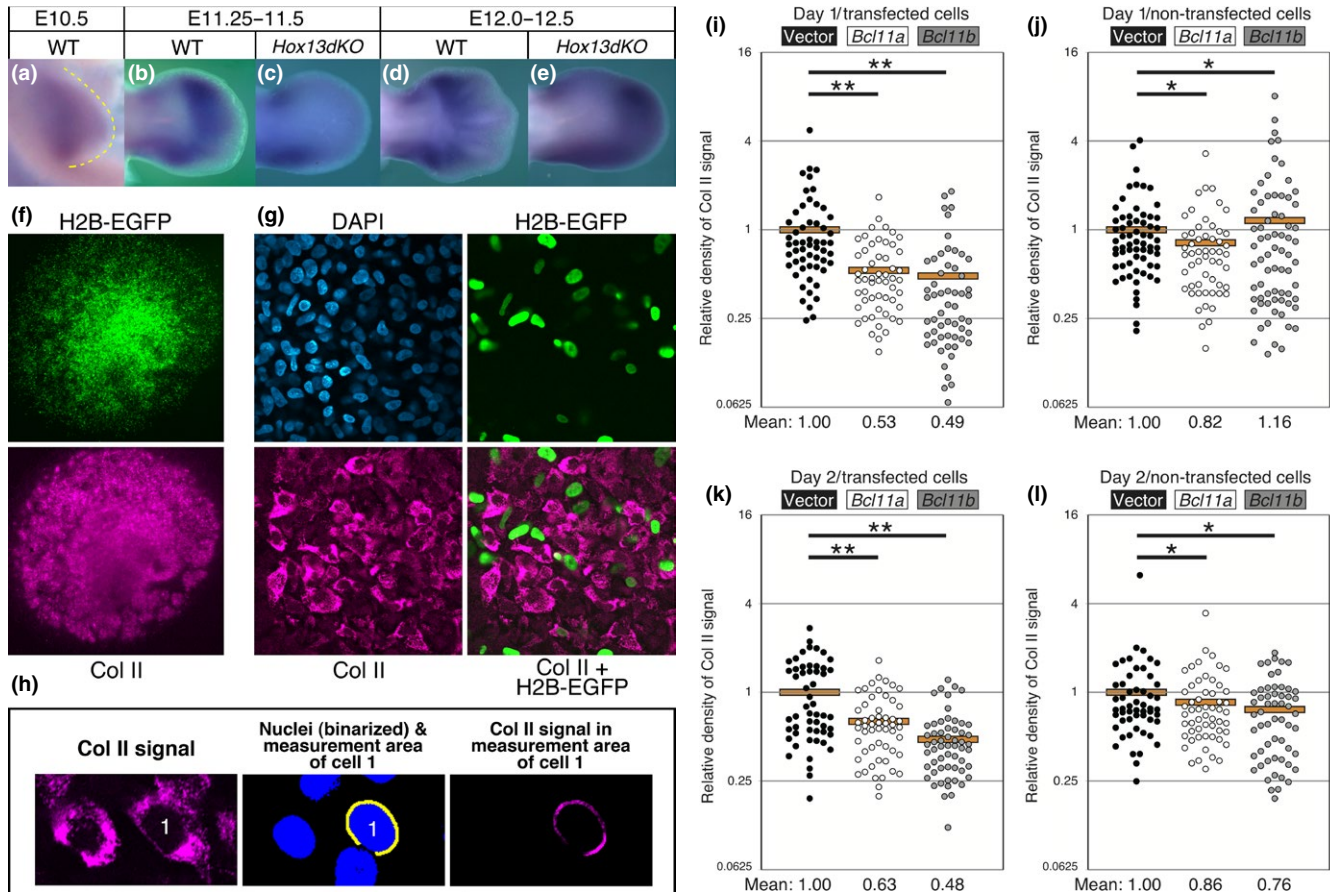

FIGURE 9 BCL11a and BCL11b repress cartilage differentiation in micromass culture (MMC). (a) *Bcl11a* was expressed throughout the entire mesenchyme of the limb bud at E10.5 then became restricted to the autopod and anterior and posterior margin of the more proximal part of the limb (b) at E11.5. *Bcl11a* expression was detected in the interdigital region (d) at E12.0. In the *Hox13*dKO limb (c) at E11.5, autopodal expression was severely reduced but (e) at E12.5 uniform expression was detected throughout the autopod. (f) Histone H2B-EGFP (H2B-EGFP) fluorescence and Col II immunofluorescence signals in MMCs incubated for 2 days after transfection with the pCAGGS-*H2B-EGFP* and pCAGGS vector. (g) High magnification confocal images of the MMC in panel f. Nuclei of the transfected cells were marked with H2B-EGFP. (h) For quantitative analyses of Col II expression in each cell, the intensity of the Col II immunofluorescence signal in the ring-shaped area (yellow; width: 0.58 μm) around each nucleus (green) was calculated using ImageJ. Neighboring nuclear areas were excluded from the measurement area. (i–l) Ratios of Col II immunofluorescence signal intensity in each cell relative to the mean of the vector transfection control. i, j: 1-day incubation; k, l: 2-day incubation. i, k: transfected cells (H2B-EGFP-positive); j, l: non-transfected cells (H2B-EGFP-negative). In the graphs, a circle represents one cell, and $n \approx 60$ for each transfection. **$p < 0.002$; *$p > 0.01$ (Mann–Whitney *U*-test). Orange bars indicate the mean of the values

also expressed. As expected from Genechip analysis, expression was severely decreased in the E11.5 autopodal mesenchyme of the *Hox13*dKO (Figure 9c). Interestingly, *Bcl11a* expression reappeared in the *Hox13*dKO autopod at E12.0 where the single flat cartilage was forming instead of the five metacarpi and phalanges (Figure 9e).

We then analyzed the effect of *Bcl11a* overexpression on the differentiation of the limb mesenchymal cells into cartilage using a micromass culture system and monitoring Col II expression as a marker of differentiation (Figure 9f–h). We also analyzed the effect of another family gene, *Bcl11b*, that is expressed in the limb mesenchyme

(result not shown) and has both HOXA11 and HOXA13 binding sites (Supporting Information Table S2). As shown in Figure 9i,j, the expression level of Col II was reduced to 53% and 49% in the *Bcl11a* and *Bcl11b* transfected cells, respectively, compared to vector-transfected cells at day 1. At day 2, the expression of Col II in *Bcl11a* and *Bcl11b* transfected cells was also reduced to 63% and 48%, respectively (Figure 9k,l). Thus, similar to blood cell differentiation, both BCL11a and BCL11b have repressive activity on the cartilage differentiation of mesenchymal cells of the limb bud. Taken together, HOXA13 represses limb cartilage differentiation at E11.5.

4 | DISCUSSION

To elucidate the mechanism controlling region-specific morphogenesis of the zeugopod and autopod, we identified direct target genes of HOXA11 and HOXA13 in the limb bud. We found that HOXA11and HOXA13 regulate their common target genes involved in cartilage differentiation in distinct way, where HOXA13-dependent regulation appears to be central to generating pentadactylous (five digits) autopod.

ChIP-Seq analysis is a technique for identification of *Hox* target genes. Using the same HOXA13 antibody as in this study, we have shown that HOXA13 regulates autopod-specific expression of *Hoxd13* through direct binding to the digit-specific enhancer (Beccari et al., 2016). Sheth et al. (Sheth et al., 2016) identified the limb target genes of HOXA13 and HOXD13, whose function is redundant in the autopodal development. They reported most of the target genes are common to both HOXA13 and HOXD13 and many of them are related to cartilage differentiation. Further extraction and elucidation of the crucial genes from these many candidate genes are current subjects. Jerkovic et al. (2017) attempted to identify the *Hox* target genes by ChIP-Seq analysis after forced expression of paralogous *Hox* genes in cultured chicken limb bud mesenchymal cells. They found that common HOX binding site and a group of HOX proteins interact with CTCF. Since this analysis was performed using cultured cells and overexpression of tagged HOX protein, the results need to be verified by using a more native system. A loss-of-function phenotype for *Hox11* was observed in the zeugopod and proximal autopod, and for *Hox13* in the autopod. In both cases, hypomorphic cartilage development was observed indicating the presence of common target genes responsible for chondrogenic differentiation from limb bud mesenchymal cells. In this study, we used mesenchymal cells from mouse limb bud and antibodies against HOXA11 or HOXA13 for our ChIP-Seq analysis to narrow down the common *Hox* target genes that are critical for chondrogenic differentiation. Based on the analysis of these target genes, we revealed the unique role of *Hox13* in the autopod-specific gene regulation network.

4.1 | HOX11/13, SHOX2 and PITX1 share common targets

We showed that most of the HOXA11 ChIP-Seq peaks overlapped with the HOXA13 peaks (Figures 2 and 3 and Supporting Information Figure S2) and many of the genes neighboring the common peak are involved in cartilage differentiation (Supporting Information Figure S6A). Since *Hoxa11* and *Hoxa13* are expressed in the zeugopod and autopod, respectively, except carpal/tarsal region (Figure 1 and Supporting Information Figure S1), each HOX11/13 binds to a common sequence in their unique expression domain and are expected to control the target gene expression in an expression domain-specific manner. In addition, non-HOX homeodomain transcription factors are shown to bind to the same region in the common HOX11/13 binding domain of the limb bud.

There is accumulating evidence that Hox and non-Hox homeodomain transcription factors coordinate during limb cartilage development. *Pitx1* encodes a paired-like homeodomain transcription factor whose expression in the limb bud is restricted to the hindlimb and functions to transform forelimb type morphogenesis to hindlimb type morphogenesis (Lanctot, Moreau, Chamberland, Tremblay, & Drouin, 1999). Both the fore- and hindlimbs have basically the same topological architecture of the bone and differences in their morphology are thought to be based on quantitative rather than qualitative variation in gene expression or temporal differences in expression of common genes functioning in the limb cartilage development. The expression of *Hox* and *Pitx1* in the mesenchyme of the hindlimb bud is largely overlapping (Shang, Luo, & Clayton, 1997). In the present study, we found many ChIP-Seq proximal genes are shared by HOX11/13 and PITX1 (Figures 2 and 3) and that many of these genes are involved in cartilage differentiation (Supporting Information Figure S6D), These indicate that PITX1 also participates in directly regulating cartilage differentiation in collaboration with HOX11/13. Since the *Hox* expression pattern in the fore- and hindlimb bud is very similar, binding of PITX1 to the HOX11/13 common binding region (CHBRLs) could modulate HOX function. One plausible molecular mechanism for the interplay between PITX1 function and HOX11/13 is that binding of PITX1 to some HBSs of multiple HBSs in the enhancer results in fine tuning of the transcriptional frequency or timing in a program characteristic to that of the hindlimb bud. Given that CHBRLs potentially include multiple HBSs (Figure 4, Supporting Information Figure S5), analysis of interaction of multiple transcription factors in combination with CHBRL sequences will provide new insights into the complex regulatory processes centered by HOX13.

Another interesting example on functional coordination with *Hox* is *Shox2* that encodes a paired-like homeodomain transcription factor. Mice with a loss of *Shox2* function exhibited severe truncation of the stylopod bone of fore- and hindlimbs in addition to hypoplasia of the hindlimb zeugopodal bone (Bobick & Cobb, 2012; Cobb et al., 2006). *Shox2* showed overlapping expression with *Hoxa9-11* in the mesenchyme of the stylopod and zeugopod then in the outer layer of the perichondrium and proliferating chondrocytes but not in the autopod (Neufeld, Wang, & Cobb, 2014; Swinehart, Schlientz, Quintanilla, Mortlock, & Wellik, 2013). Genetic analysis revealed that *Shox2* is a downstream gene of *Hox11* (Gross, Krause, Wuelling, & Vortkamp, 2012). We found that HOXA11 binds to one of the *Shox2* limb-specific enhancers (Supporting Information Figure S2C

and Figure 4) indicating the possibility that HOXA11 directly control region-specific expression of *Shox2* in the limb buds through binding to this enhancer/CHBRL. HOXA13 also binds this CHBRL (Supporting Information Figure S2C and Figure 4) and *Shox2* is mis-expressed in the *Hox13*dKO (Figure 6g,h) suggesting that binding of HOXA13 to this enhancer is involved in repressing *Shox2* expression in the autopod. SHOX2 also bind to this CHBRL (Supporting Information Figure S2C) indicating that SHOX2 participate self-regulation in coordination with HOX11. Interestingly, genetic analysis also suggested that *Hox* and *Shox2* coordinate during development of the stylopodal and zeugopodal cartilage (Neufeld et al., 2014). Supporting this observation, we showed that SHOX2 also shares common binding regions of some *Hox* target genes with HOXA11 and HOXA13 (Figures 2 and 3, Supporting Information Figure S2 and Table S2). Genes involved in the skeletal development, such as *Aff3*, *Bmp2*, *Bnc2* and *Runx1t1* were concentrated in these common genes (Supporting Information Figure S6B). These indicate the possibility that SHOX2 and HOXA11 coordinately regulate these gene expression through the CHBRLs in the zeugopod by the similar mechanism as the PITX1 and HOXA11. Thus, HOXs regulate multiple steps in the SHOX2 functional cascade during cartilage development along the proximodistal axis of the limb.

4.2 | On the HOX binding to the *Hoxa11* intron

The binding profiles of HOXA11, HOXA13 and other homeodomain transcription factors to the HoxA cluster are different (Figure 2a). Both HOXA11 and HOXA13 bind to the 5′ untranslated region (5′-UTR) of the *Hoxa9* and *Hoxa7* intron. However, while HOXA13 binds to the *Hoxa11* intronic region, the binding of HOXA11 to the *Hoxa11* intron is minimal or negligible (Figure 2a). This indicates that in the autopod, HOXA13 binds to the *Hoxa11* intron but HOXA11 shows little or no binding to the *Hoxa11* intron in the zeugopodal anlage. *Hoxc10* is expressed in the mesenchyme of the stylopodal and zeugopodal anlagen of the hindlimb bud. Using deposited ChIP-Seq data (Jain et al., 2018), we found that HOXC10 also binds to the *Hoxa7* intron and *Hoxa9* 5′-UTR but binding to the *Hoxa11* intron was significantly lower or indistinguishable from background (Supporting Information Figure S10). Interestingly, non-HOX homeodomain transcription factors SHOX2 and PBX also exhibited similar binding profiles to the *Hoxa11* intron (Figure 2a). HOXA13 and HOXD13 bind to the "digit enhancer" in the *Hoxa11* intron and activate transcription from the promoter in the first exon of *Hoxa11* in the opposite direction as *Hoxa11* transcription. This counter directional transcription itself is important to inactivate *Hoxa11* transcription in the autopod (Kherdjemil et al., 2016). Based on the observation that *Hoxa11* and *Hoxa13* are co-expressed in the distal fin bud of fish and that forced mis-expression of *Hoxa11* in the autopodal anlage in the mouse causes polydactyly, the system that represses *Hoxa11* expression in the autopod of tetrapods is expected to have been acquired during the evolutionary transition from polydactyly to pentadactyly (Kherdjemil et al., 2016). Like most of the CHBRL, multiple and evolutionarily conserved HBSs are present in the *Hoxa11* intronic "digital

enhancer" (Supporting Information Figure S11). As described, compared to other common HOX11/13 binding regions, the binding to the *Hoxa11* intron is very specific to HOXA13. It is possible that novel transcriptional co-factor(s) specifically interacts with HOXA13 to stabilize HOXA13 binding to the HBS(s) in the *Hoxa11* intronic "digital enhancer". These suggest that in addition to the recruitment of the HOX binding sequence itself to the *Hoxa11* intron, the system whereby homeodomain transcription factor binding to the *Hoxa11* intron is restricted to HOXA13 was likely also introduced during the evolutionary transition from polydactyly to pentadactyly.

4.3 | The role of multiple HBSs in CHBRLs

We showed that the sequences and the presence of multiple HBSs in most of the common ChIP-peaks of HOXA11 and HOXA13 (CHBRLNr) are evolutionarily conserved among tetrapods (Supporting Information Figures S5 and S11). The representative fragments exhibited direct binding of HOXA11 and HOXA13 to multiple binding sites *in vitro* (Figure 4 and Supporting Information Figure S5) indicating that these HOX members may have similar binding profiles *in vivo*. Different from HOX1-10, HOXA11 and HOXA13 can bind to the target sequence without the co-factor homeodomain transcription factor, PBXs (Shen et al., 1997), and most of the conserved HBSs in the CHBRLNr do not neighbor the consensus PBX binding sequence. Thus, it is likely that HOXA11 and HOXA13 solely bind their target sites. Since the clustered low affinity HBSs guarantee specificity and robustness of HOX binding in *Drosophila* (Crocker et al., 2015), multiple HOXA11 and HOXA13 binding sites in the vertebrate CHBRLNr should have the same role. This possibility is also supported by evidence that *Abd-B Hox* function shows a dosage effect on the patterning of limb cartilage (Zakany et al., 1997).

4.4 | HOX function in the carpal/tarsal region

As already described, the relationship in the expression profile of *Hoxa11* and *Hoxa13* is unique. *Abd-B* family genes in the *HoxD* cluster, *Hoxd9-13*, maintain overlapping expression patterns in the limb bud, although transcription of *Hoxa11* is repressed in the distal limb bud by HOXA13 function. However, in the proximal region of the carpal/tarsal anlage, *Hoxa11* and *Hoxa13* maintain their co-expression despite the prominent expression of *Hoxa13* in the autopodal anlage (Figure 1 and Supporting Information Figure S1). Loss-of-function of either *Hoxa11* or *Hoxd11* also results in abnormal formation of the carpal/tarsal bones, similar to *Hox13* mutations indicating that *Hox11* has an additional role in the morphogenesis of the autopod other than just the zeugopod (Davis & Capecchi, 1994; Fromental-Ramain et al., 1996; Small & Potter, 1993). Cartilage formation in the carpal/tarsal region is unique compared to other limb regions. As shown in Figure 1 and Supporting Information Figure S1, initially *Col2a1* expressing precartilaginous rudiment is formed in the prospective carpal/tarsal region, then multiple dense and small precartilaginous condensations individualize as an archipelago. These precartilaginous condensations develop into cartilage and maintain the cartilaginous

state for much longer than other regions and never develop into long bones. In contrast, in the prospective long bone forming regions, *Hoxa11* and *Hoxa13* exhibit mutually exclusive expression. It is possible that HOXA11 and HOXA13 co-exist in the regulatory region of the target gene carrying multiple HBSs in the carpal/tarsal anlage. This unique mixed state may enable the unique mode of cartilage differentiation in the carpal/tarsal region. We have previously shown that mis-expression of *Hoxa13* in the zeugopodal region results in the transformation of the zeugopodal cartilage into the carpal/tarsal-like cartilage (Yokouchi et al., 1995), and this evidence further supports the hypothesis.

4.5 | Regulation of *Hox* target genes by HOX

We identified the genes neighboring the CHBRLNr and demonstrated that their expression is changed in *Hox13*dKO embryos (Figures 6, 7 and 9 and Supporting Information Figure S9), thus confirming them to be direct *Hox* target genes. These genes are classified into two groups according to the changes in their mRNA levels in the *Hox13*dKO autopod. The genes in the first group showed reduced mRNA levels in the *Hox13*dKO, indicating that HOXA13 activates their transcription. The genes in the second group showed increased mRNA levels in the *Hox13*dKO and are likely repressed by HOXA13 during normal development.

Bmp2, *Sulf1* and *Stmn2* belong to the first group, and are expressed in the autopodal mesenchyme in wild-type animals and exhibited a substantial reduction in expression levels in the *Hox13*dKO embryos (Figure 6 and Supporting Information Figure S9). In the case of second gene group, expression of *Aff3*, *Bnc2*, *Nfib*, *Runx1t1*, *Shox2* and *Tshz2* are restricted to the zeugopodal mesenchyme of the wild-type embryos at E11.25–11.5, but showed ectopic expression in the autopod mesenchyme of *Hox13*dKO embryos (Figure 6 and Supporting Information Figure S9). Interestingly, the ectopic expression of *Aff3*, *Bnc2*, *Nfib* and *Runx1t1* was uniform in the *Hox13*dKO autopod, whereas *Shox2* mis-expression was restricted to a narrow posterior region of the *Hox13*dKO autopod and *Tshz2* mis-expression was only found in the distal autopod. These results indicate the presence of various mechanisms for HOXA13 negative regulation of downstream genes.

The expression of *Hox* target genes, *Aff3*, *Bnc2* and *Nfib* is induced during cartilage differentiation, consistent with their known roles in cartilage differentiation (Steichen-Gersdorf et al., 2008; Uchihashi et al., 2007; Vanhoutteghem et al., 2009). As discussed above, the expression of these genes was not detected in the E11.5 autopodal anlage. Interestingly, these genes become expressed in the autopodal cartilage or perichondrium at E12.5 and sometimes even show partial overlapping expression with *Hoxa13*. Thus, repression of these genes by HOXA13 in the autopodal mesenchyme is transient during autopodal cartilage development. From E11.5 to E12.5 metacarpal/metatarsal and digital cartilage formation progresses distally and mesenchymal *Hoxa13* expression gradually decreases and disappears in the cartilage. During this period, in addition to the decreased amounts of HOXA13 protein, changes in the regulatory activity of HOXA13

may occur by modification of HOXA13 itself or by *de novo* induction of the HOXA13 co-factors that alter its transcriptional activity. Alternatively, since HOXA13 does not always bind to the H3K27ac enriched region of HOXA13 target genes, transitional usage of the enhancer may occur between HOXA13 dependent regulatory elements and independent elements during cartilage differentiation from the limb mesenchyme. Enhancer switching during development has previously been demonstrated (Andrey et al., 2013; Beccari et al., 2016; Glasgow et al., 2017), thus it is possible that a similar system is employed during cartilage differentiation.

In contrast to autopodal expression, these *Hox* target genes are also expressed in the zeugopodal mesenchyme prior to their cartilage expression and exhibit nearly complete overlap with *Hoxa11* expression. This suggests that the mechanisms underlying HOXA11-dependent and HOXA13-dependent gene regulations are different.

4.6 | HOX13 regulates cartilage differentiation in a dual manner

In contrast to the genes encoding transcription factors that are enriched among the *Hox* targets with upregulated expression in the *Hox13*dKO limb bud (Supporting Information Figure S8), relatively few *Hox* target transcription factors were identified in the downregulated fraction (Supporting Information Figure S8). A typical example of the latter case is *Bcl11a*. *Bcl11a* encodes a zinc finger-type transcription factor and functions as a repressor during blood cell differentiation (Liu et al., 2003). We found that *Bcl11a* along with its family member *Bcl11b*, repressed cartilage differentiation from the limb bud mesenchyme (Figure 9).

In the *Hox13*dKO autopod, the entire autopodal mesenchyme excluding the distal most region, enters the cartilage differentiation pathway earlier than during normal development. *Bcl11a* is expressed in the autopodal mesenchyme in the wild-type E11.5 embryos and its expression is substantially reduced in the *Hox13*dKO limb bud (Figure 9b,c). This indicates that the cartilage differentiation program repressed by HOXA13 is de-repressed in the *Hox13*dKO autopod. Simultaneously, the *Hox* target transcription factors whose expression is induced during cartilage differentiation, are mis-expressed in the mesenchyme of the *Hox13*dKO autopodal anlage. Combined, these results indicate that HOXA13 simultaneously activates the expression of repressive transcription factors for chondrogenesis (BCL11A) and represses the expression of transcription factors required to induce chondrogenesis in the autopod at E11.5. This demonstrates the presence of a dual regulatory mechanism for chondrogenesis during normal autopod development under the control of *Hoxa13*. In contrast to the autopod, *Hoxa11* and *Hox* target genes such as *Aff3*, *Bnc2*, *Nfib*, Shox2 and *Runx1t1*, are co-expressed in the zeugopodal mesenchyme. This implies that, different from HOXA13, HOXA11 does not repress the expression of these target genes. Thus, the HOXA13-dependent dual control system is autopod-specific.

Regarding the genes not expressed in the autopodal mesenchyme at E11.5 but that are mis-expressed in the *Hox13*dKO, we proposed that HOXA13 may repress these genes during normal development.

However, the following mechanism is equally probable; for these target genes, HOX13 may function as a weaker transcriptional activator than HOX11. The evidence that limb mesenchymal cells isolated from Hoxa13$^{-/-}$ embryos did not show cartilage differentiation *in vitro* support that HOXA13 is required for cartilage differentiation (Stadler, Higgins, & Capecchi, 2001). If repressive transcription factor(s) for the *Hox* target gene expression are present in the E11.5 autopodal mesenchyme, and transcriptional activation by HOX13 does not overcome this repressive activity, the autopodal expression of the *Hox* target gene does not occur. *Hoxa11* and *Hoxa13* exhibited mutually exclusive expression in the limb bud except in the carpal/tarsal anlage; however, in the *Hox13*dKO autopod, *Hoxa11* expression is expanded to the autopodal mesenchyme (Sheth, Bastida, Kmita, & Ros, 2014). This ectopic HOXA11 may mis-activate the common *Hox* target genes required for cartilage differentiation in the *Hox13*dKO autopod. The evidence that the forced mis-expression of *Hoxa11* in the autopod results in polydactyly supports this possibility (Kherdjemil et al., 2016). Expression analysis of common *Hox* target genes in the autopod under *Hoxa11* mis-expression may help to verify this mechanism.

The molecular mechanism that is responsible for the dual transcriptional activity of HOXA13 presented here, along with the similar effect of HOXA13 on *HoxD* gene expression shown by Beccari et al. (Beccari et al., 2016), remains elusive. Recently it is reported that a transcription factor that shows unique spatiotemporal expression patterns, interacts with HOX in a DNA binding dependent or independent manner, then modulates the function of HOX transcription factors (Guerreiro et al., 2013). In the case of *Drosophila*, the phosphorylation state of the HOX protein is crucial for its transcriptional activity (Berry & Gehring, 2000). In addition, the presence of the co-factors that modulate transcriptional activity of *Drosophila* HOX was reported (reviewed in Zandvakili & Gebelein, 2016). Since these mechanisms related to HOXA13 have yet to be elucidated, research into this issue will be a topic for future studies.

4.7 | *Hox13* controls tetrapod specific autopodal structure

Why does *Hoxa13*, the last member of the *HoxA* cluster, have such unique function compared to other *Hox* genes expressed in the zeugopod or stylopod? This is likely related to the development of tetrapod-specific autopodal structures. In contrast to the zeugopod and stylopod, the autopod generally consists of five sets of long bones, the metacarpi/metatarsi and phalanges (pentadactyly). One
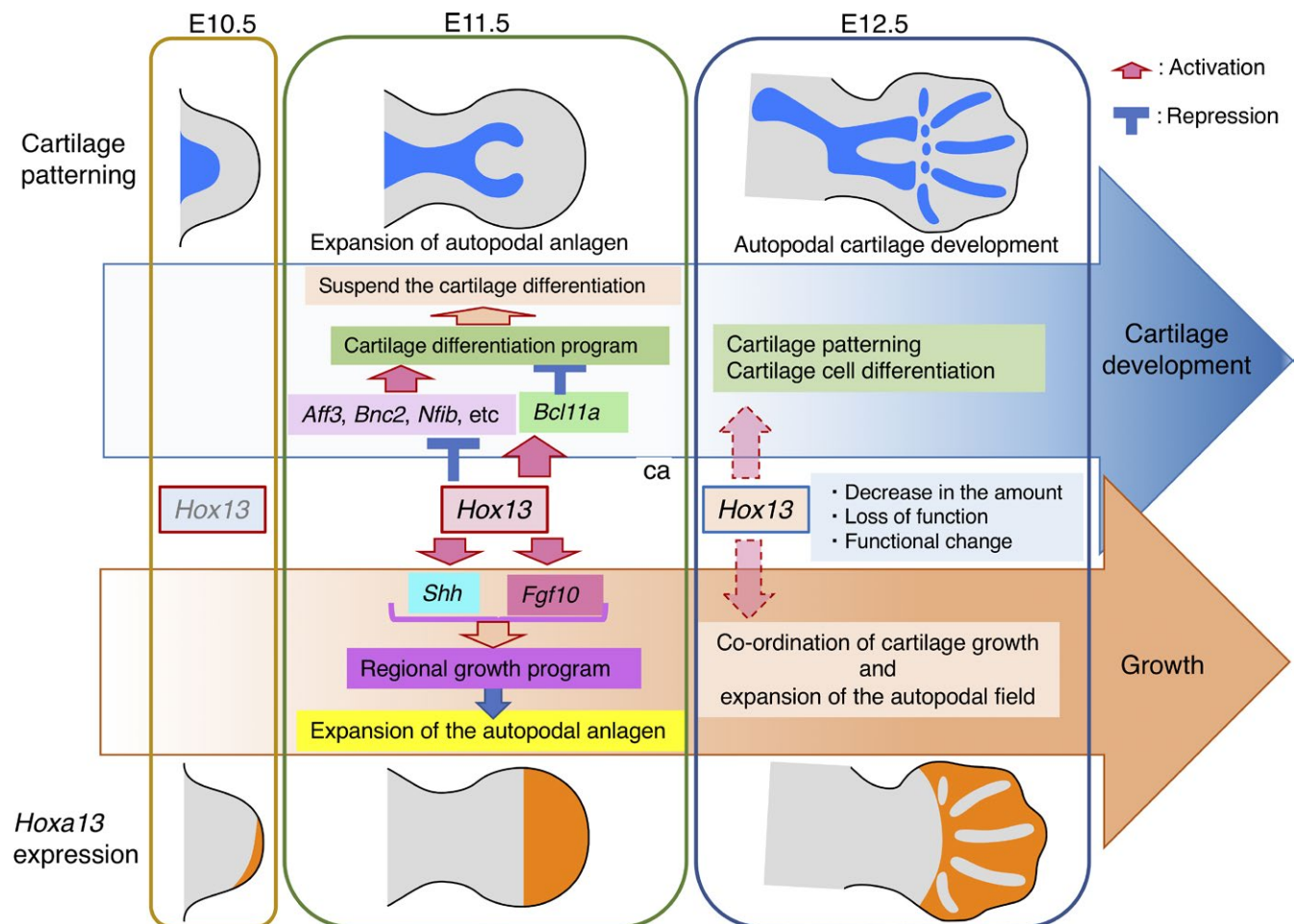

FIGURE 10 Dynamic change in the *Hoxa13* function during autopod development

and two long bones exist in the stylopod and zeugopod, respectively, and the shape of their prospective region in the limb bud is a nearly elliptical cylinder. In contrast, the autopodal anlage has a unique paddle-shaped structure that is required for supplying a sufficient number of mesenchymal cells to generate the pentadactylous cartilage pattern. The signaling factor, SHH, expressed in the mesenchyme of the posterior limb bud, is essential for expansion of the autopodal anlage (Chiang et al., 1996) and *Hox13* directly activates *Shh* expression via a limb enhancer (Leal & Cohn, 2016, 2018). In addition, another signaling molecule, *Fgf10*, expressed in the distal limb bud, is required for limb bud formation and growth (Sekine et al., 1999). *Abd-B Hox* is also involved in activating *Fgf10* expression in the limb bud (Sheth et al., 2013) and we found that HOXA11 and HOXA13 bind one of the *Fgf10* limb enhancers (VISTA ID mm917, Supporting Information Table S2). Thus, *Hox13* positively controls the proliferation of autopodal mesenchymal cells to supply sufficient number of mesenchymal cells to generate the pentadactylous autopodal cartilage pattern. As discussed above, HOX13 transiently represses the cartilage differentiation program in the autopodal anlage in a dual manner. Thus, *Hox13* functions on one hand to control the autopod-specific growth program to supply enough mesenchyme and, on the other hand, transiently represses the cartilage forming program until the mesenchymal supply reaches a sufficient level to form pentadactylous structures (Figure 10).

The pentadactylous autopodal architecture is unique to the tetrapods and this basic architectural design was key to tetrapod evolution through niche diversification. Recently, in fish, *Hox13* genes were shown to function in switching the fin bud mesenchymal developmental program from cartilage formation to fin ray differentiation (Nakamura, Gehrke, Lemberg, Szymaszek, & Shubin, 2016). In the case of pentadactylous tetrapods, *Hox13* function switched from the fish program to the tetrapod-specific autopod-forming program, possibly through the acquisition of the dual control system for cartilage differentiation.

ACKNOWLEDGMENTS

AUTHOR CONTRIBUTIONS

SY, YU, YG and NK: ChIP-Seq; TO: Genechip and WISH, SY, YS, EN and CY: WISH; TH and TS: NGS analysis; TT: enhancer knock out; YS: *Bcl11a,b* study; YS and AK: management of the project; AK: planning of the project, bioinformatic analysis and manuscript writing.

ORCID

Atsushi Kuroiwa (iD) https://orcid.org/0000-0001-7710-4041

REFERENCES

Andrey, G., Montavon, T., Mascrez, B., Gonzalez, F., Noordermeer, D., Leleu, M., ... Duboule, D. (2013). A switch between topological domains underlies HoxD genes collinearity in mouse limbs. *Science*, *340*, 1234167. https://doi.org/10.1126/science.1234167

Beccari, L., Yakushiji-Kaminatsui, N., Woltering, J. M., Necsulea, A., Lonfat, N., Rodriguez-Carballo, E., ... Duboule, D. (2016). A role for HOX13 proteins in the regulatory switch between TADs at the HoxD locus. *Genes & Development*, *30*, 1172–1186.

Berry, M., & Gehring, W. (2000). Phosphorylation status of the SCR homeodomain determines its functional activity: Essential role for protein phosphatase 2A, B'. *EMBO Journal*, *19*, 2946–2957. https://doi.org/10.1093/emboj/19.12.2946

Bobick, B. E., & Cobb, J. (2012). Shox2 regulates progression through chondrogenesis in the mouse proximal limb. *Journal of Cell Science*, *125*, 6071–6083. https://doi.org/10.1242/jcs.111997

Boulet, A. M., & Capecchi, M. R. (2004). Multiple roles of Hoxa11 and Hoxd11 in the formation of the mammalian forelimb zeugopod. *Development*, *131*, 299–309.

Buscher, D., Bosse, B., Heymer, J., & Ruther, U. (1997). Evidence for genetic control of Sonic hedgehog by Gli3 in mouse limb development. *Mechanisms of Development*, *62*, 175–182. https://doi.org/10.1016/s0925-4773(97)00656-4

Capellini, T. D., Di Giacomo, G., Salsi, V., Brendolan, A., Ferretti, E., Srivastava, D., ... Selleri, L. (2006). Pbx1/Pbx2 requirement for distal limb patterning is mediated by the hierarchical control of Hox gene spatial distribution and Shh expression. *Development*, *133*, 2263–2273. https://doi.org/10.1242/dev.02395

Caubit, X., Core, N., Boned, A., Kerridge, S., Djabali, M., & Fasano, L. (2000). Vertebrate orthologues of the *Drosophila* region-specific patterning gene teashirt. *Mechanisms of Development*, *91*, 445–448. https://doi.org/10.1016/s0925-4773(99)00318-4

Chen, Y., Knezevic, V., Ervin, V., Hutson, R., Ward, Y., & Mackem, S. (2004). Direct interaction with Hoxd proteins reverses Gli3-repressor function to promote digit formation downstream of Shh. *Development*, *131*, 2339–2347. https://doi.org/10.1242/dev.01115

Chiang, C., Litingtung, Y., Lee, E., Young, K. E., Corden, J. L., Westphal, H., & Beachy, P. A. (1996). Cyclopia and defective axial patterning in mice lacking Sonic hedgehog gene function. *Nature*, *383*, 407–413. https://doi.org/10.1038/383407a0

Cobb, J., Dierich, A., Huss-Garcia, Y., & Duboule, D. (2006). A mouse model for human short-stature syndromes identifies Shox2 as an upstream regulator of Runx2 during long-bone development. *Proceedings of the National Academy of Sciences of the United States of America*, *103*, 4511–4515. https://doi.org/10.1073/pnas.0510544103

Crocker, J., Abe, N., Rinaldi, L., McGregor, A. P., Frankel, N., Wang, S., ... Stern, D. L. (2015). Low affinity binding site clusters confer hox specificity and regulatory robustness. *Cell*, *160*, 191–203. https://doi.org/10.1016/j.cell.2014.11.041

Dathe, K., Kjaer, K. W., Brehm, A., Meinecke, P., Nurnberg, P., Neto, J. C., ... Mundlos, S. (2009). Duplications involving a conserved regulatory

element downstream of BMP2 are associated with brachydactyly type A2. *American Journal of Human Genetics*, *84*, 483–492. https://doi.org/10.1016/j.ajhg.2009.03.001

Davis, A. P., & Capecchi, M. R. (1994). Axial homeosis and appendicular skeleton defects in mice with a targeted disruption of hoxd-11. *Development*, *120*, 2187–2198.

Davis, A. P., Witte, D. P., Hsieh-Li, H. M., Potter, S. S., & Capecchi, M. R. (1995). Absence of radius and ulna in mice lacking hoxa-11 and hoxd-11. *Nature*, *375*, 791–795. https://doi.org/10.1038/375791a0

Dickinson, M. E., Kobrin, M. S., Silan, C. M., Kingsley, D. M., Justice, M. J., Miller, D. A., ... Jenkins, N. A. (1990). Chromosomal localization of seven members of the murine TGF-beta superfamily suggests close linkage to several morphogenetic mutant loci. *Genomics*, *6*, 505–520. https://doi.org/10.1016/0888-7543(90)90480-i

Fromental-Ramain, C., Warot, X., Messadecq, N., LeMeur, M., Dolle, P., & Chambon, P. (1996). Hoxa-13 and Hoxd-13 play a crucial role in the patterning of the limb autopod. *Development*, *122*, 2997–3011.

Giardine, B., Riemer, C., Hardison, R. C., Burhans, R., Elnitski, L., Shah, P., ... Nekrutenko, A. (2005). Galaxy: A platform for interactive large-scale genome analysis. *Genome Research*, *15*, 1451–1455. https://doi.org/10.1101/gr.4086505

Gilbert, S. F., & Barresi, M. J. F. (2016). *Developmental biology*. Sunderland, MA: Sinauer Associates, Inc.

Glasgow, S. M., Carlson, J. C., Zhu, W., Chaboub, L. S., Kang, P., Lee, H. K., ... Deneen, B. (2017). Glia-specific enhancers and chromatin structure regulate NFIA expression and glioma tumorigenesis. *Nature Neuroscience*, *20*, 1520–1528. https://doi.org/10.1038/nn.4638

Goff, D. J., & Tabin, C. J. (1997). Analysis of Hoxd-13 and Hoxd-11 misexpression in chick limb buds reveals that Hox genes affect both bone condensation and growth. *Development*, *124*, 627–636.

Green, M. R., & Sambrook, J. (Eds.) (2012). *Molecular cloning: A laboratory manual*, 4th edn. Cold Spring Harbor, NY: Cold Spring Harbor Laboratory Press.

Gross, S., Krause, Y., Wuelling, M., & Vortkamp, A. (2012). Hoxa11 and Hoxd11 regulate chondrocyte differentiation upstream of Runx2 and Shox2 in mice. *PLoS ONE*, *7*, e43553. https://doi.org/10.1371/journal.pone.0043553

Guerreiro, I., Nunes, A., Woltering, J. M., Casaca, A., Novoa, A., Vinagre, T., ... Mallo, M. (2013). Role of a polymorphism in a Hox/Pax-responsive enhancer in the evolution of the vertebrate spine. *Proceedings of the National Academy of Sciences of the United States of America*, *110*, 10682–10686. https://doi.org/10.1073/pnas.1300592110

Hashimoto, M., Yamashita, Y., & Takemoto, T. (2016). Electroporation of Cas9 protein/sgRNA into early pronuclear zygotes generates non-mosaic mutants in the mouse. *Developmental Biology*, *418*, 1–9. https://doi.org/10.1016/j.ydbio.2016.07.017

Huang da, W., Sherman, B. T., & Lempicki, R. A. (2009). Systematic and integrative analysis of large gene lists using DAVID bioinformatics resources. *Nature Protocols*, *4*, 44–57. https://doi.org/10.1038/nprot.2008.211

Izpisua-Belmonte, J. C., Tickle, C., Dolle, P., Wolpert, L., & Duboule, D. (1991). Expression of the homeobox Hox-4 genes and the specification of position in chick wing development. *Nature*, *350*, 585–589. https://doi.org/10.1038/350585a0

Jain, D., Nemec, S., Luxey, M., Gauthier, Y., Bemmo, A., Balsalobre, A., & Drouin, J. (2018). Regulatory integration of Hox factor activity with T-box factors in limb development. *Development*, *145*, dev159830. https://doi.org/10.1242/dev.159830

Jerkovic, I., Ibrahim, D. M., Andrey, G., Haas, S., Hansen, P., Janetzki, C., ... Mundlos, S. (2017). Genome-wide binding of posterior HOXA/D transcription factors reveals subgrouping and association with CTCF. *PLoS Genetics*, *13*, e1006567. https://doi.org/10.1371/journal.pgen.1006567

Karolchik, D., Hinrichs, A. S., Furey, T. S., Roskin, K. M., Sugnet, C. W., Haussler, D., & Kent, W. J. (2004). The UCSC table browser data retrieval tool. *Nucleic Acids Research*, *32*, D493–D496. https://doi.org/10.1093/nar/gkh103

Kherdjemil, Y., Lalonde, R. L., Sheth, R., Dumouchel, A., de Martino, G., Pineault, K. M., ... Kmita, M. (2016). Evolution of Hoxa11 regulation in vertebrates is linked to the pentadactyl state. *Nature*, *539*, 89–92. https://doi.org/10.1038/nature19813

Kmita, M., Tarchini, B., Zakany, J., Logan, M., Tabin, C. J., & Duboule, D. (2005). Early developmental arrest of mammalian limbs lacking HoxA/HoxD gene function. *Nature*, *435*, 1113–1116. https://doi.org/10.1038/nature03648

Lanctot, C., Moreau, A., Chamberland, M., Tremblay, M. L., & Drouin, J. (1999). Hindlimb patterning and mandible development require the Ptx1 gene. *Development*, *126*, 1805–1810.

Langmead, B., & Salzberg, S. L. (2012). Fast gapped-read alignment with Bowtie 2. *Nature Methods*, *9*, 357–359. https://doi.org/10.1038/nmeth.1923

Leal, F., & Cohn, M. J. (2016). Loss and Re-emergence of legs in snakes by modular evolution of sonic hedgehog and HOXD enhancers. *Current Biology*, *26*, 2966–2973. https://doi.org/10.1016/j.cub.2016.09.020

Leal, F., & Cohn, M. J. (2018). Developmental, genetic, and genomic insights into the evolutionary loss of limbs in snakes. *Genesis*, *56*, e23077. https://doi.org/10.1002/dvg.23077

Lewandowski, J. P., Du, F., Zhang, S., Powell, M. B., Falkenstein, K. N., Ji, H., & Vokes, S. A. (2015). Spatiotemporal regulation of GLI target genes in the mammalian limb bud. *Developmental Biology*, *406*, 92–103. https://doi.org/10.1016/j.ydbio.2015.07.022

Liu, P., Keller, J. R., Ortiz, M., Tessarollo, L., Rachel, R. A., Nakamura, T., ... Copeland, N. G. (2003). Bcl11a is essential for normal lymphoid development. *Nature Immunology*, *4*, 525–532. https://doi.org/10.1038/ni925

Long, H. K., Prescott, S. L., & Wysocka, J. (2016). Ever-changing landscapes: Transcriptional enhancers in development and evolution. *Cell*, *167*, 1170–1187. https://doi.org/10.1016/j.cell.2016.09.018

Machanick, P., & Bailey, T. L. (2011). MEME-ChIP: Motif analysis of large DNA datasets. *Bioinformatics*, *27*, 1696–1697. https://doi.org/10.1093/bioinformatics/btr189

McCabe, C. D., & Innis, J. W. (2005). A genomic approach to the identification and characterization of HOXA13 functional binding elements. *Nucleic Acids Research*, *33*, 6782–6794. https://doi.org/10.1093/nar/gki979

McLean, C. Y., Bristor, D., Hiller, M., Clarke, S. L., Schaar, B. T., Lowe, C. B., ... Bejerano, G. (2010). GREAT improves functional interpretation of cis-regulatory regions. *Nature Biotechnology*, *28*, 495–501. https://doi.org/10.1038/nbt.1630

Mi, H., Muruganujan, A., & Thomas, P. D. (2013). PANTHER in 2013: Modeling the evolution of gene function, and other gene attributes, in the context of phylogenetic trees. *Nucleic Acids Research*, *41*, D377–D386.

Nakamura, T., Gehrke, A. R., Lemberg, J., Szymaszek, J., & Shubin, N. H. (2016). Digits and fin rays share common developmental histories. *Nature*, *537*, 225–228. https://doi.org/10.1038/nature19322

Nemec, S., Luxey, M., Jain, D., Huang Sung, A., Pastinen, T., & Drouin, J. (2017). Pitx1 directly modulates the core limb development program to implement hindlimb identity. *Development*, *144*, 3325–3335. https://doi.org/10.1242/dev.154864

Neufeld, S. J., Wang, F., & Cobb, J. (2014). Genetic interactions between Shox2 and Hox genes during the regional growth and development of the mouse limb. *Genetics*, *198*, 1117–1126. https://doi.org/10.1534/genetics.114.167460

Oki, S., Maehara, K., Ohkawa, Y., & Meno, C. (2014). SraTailor: graphical user interface software for processing and visualizing ChIP-seq data. *Genes Cells*, *19*, 919–926. https://doi.org/10.1111/gtc.12190

Osterwalder, M., Barozzi, I., Tissieres, V., Fukuda-Yuzawa, Y., Mannion, B. J., Afzal, S. Y., ... Pennacchio, L. A. (2018). Enhancer redundancy

provides phenotypic robustness in mammalian development. *Nature*, *554*, 239–243. https://doi.org/10.1038/nature25461

Peichel, C. L., Prabhakaran, B., & Vogt, T. F. (1997). The mouse Ulnaless mutation deregulates posterior HoxD gene expression and alters appendicular patterning. *Development*, *124*, 3481–3492.

Pineault, K. M., & Wellik, D. M. (2014). Hox genes and limb musculoskeletal development. *Current Osteoporosis Reports*, *12*, 420–427. https://doi.org/10.1007/s11914-014-0241-0

Quinlan, A. R., & Hall, I. M. (2010). BEDTools: A flexible suite of utilities for comparing genomic features. *Bioinformatics*, *26*, 841–842. https://doi.org/10.1093/bioinformatics/btq033

Ramirez, F., Ryan, D. P., Gruning, B., Bhardwaj, V., Kilpert, F., Richter, A. S., … Manke, T. (2016). deepTools2: A next generation web server for deep-sequencing data analysis. *Nucleic Acids Research*, *44*, W160–W165. https://doi.org/10.1093/nar/gkw257

Robinson, J. T., Thorvaldsdottir, H., Winckler, W., Guttman, M., Lander, E. S., Getz, G., & Mesirov, J. P. (2011). Integrative genomics viewer. *Nature Biotechnology*, *29*, 24–26. https://doi.org/10.1038/nbt.1754

Rosin, J. M., Abassah-Oppong, S., & Cobb, J. (2013). Comparative transgenic analysis of enhancers from the human SHOX and mouse Shox2 genomic regions. *Human Molecular Genetics*, *22*, 3063–3076. https://doi.org/10.1093/hmg/ddt163

Salsi, V., & Zappavigna, V. (2006). Hoxd13 and Hoxa13 directly control the expression of the EphA7 Ephrin tyrosine kinase receptor in developing limbs. *Journal of Biological Chemistry*, *281*, 1992–1999. https://doi.org/10.1074/jbc.m510900200

Sekine, K., Ohuchi, H., Fujiwara, M., Yamasaki, M., Yoshizawa, T., Sato, T., … Kato, S. (1999). Fgf10 is essential for limb and lung formation. *Nature Genetics*, *21*, 138–141. https://doi.org/10.1038/5096

Selleri, L., Depew, M. J., Jacobs, Y., Chanda, S. K., Tsang, K. Y., Cheah, K. S., … Cleary, M. L. (2001). Requirement for Pbx1 in skeletal patterning and programming chondrocyte proliferation and differentiation. *Development*, *128*, 3543–3557.

Shang, J., Luo, Y., & Clayton, D. A. (1997). Backfoot is a novel homeobox gene expressed in the mesenchyme of developing hind limb. *Developmental Dynamics*, *209*, 242–253. https://doi.org/10.1002/(issn)1097-0177

Shen, W. F., Rozenfeld, S., Lawrence, H. J., & Largman, C. (1997). The Abd-B-like Hox homeodomain proteins can be subdivided by the ability to form complexes with Pbx1a on a novel DNA target. *Journal of Biological Chemistry*, *272*, 8198–8206. https://doi.org/10.1074/jbc.272.13.8198

Sheth, R., Barozzi, I., Langlais, D., Osterwalder, M., Nemec, S., Carlson, H. L., … Kmita, M. (2016). Distal limb patterning requires modulation of cis-regulatory activities by HOX13. *Cell Reports*, *17*, 2913–2926. https://doi.org/10.1016/j.celrep.2016.11.039

Sheth, R., Bastida, M. F., Kmita, M., & Ros, M. (2014). "Self-regulation", a new facet of Hox genes' function. *Developmental Dynamics*, *243*, 182–191. https://doi.org/10.1002/dvdy.24019

Sheth, R., Gregoire, D., Dumouchel, A., Scotti, M., Pham, J. M., Nemec, S., … Kmita, M. (2013). Decoupling the function of Hox and Shh in developing limb reveals multiple inputs of Hox genes on limb growth. *Development*, *140*, 2130–2138. https://doi.org/10.1242/dev.089409

Shin, H., Liu, T., Manrai, A. K., & Liu, X. S. (2009). CEAS: Cis-regulatory element annotation system. *Bioinformatics*, *25*, 2605–2606. https://doi.org/10.1093/bioinformatics/btp479

Small, K. M., & Potter, S. S. (1993). Homeotic transformations and limb defects in Hox A11 mutant mice. *Genes & Development*, *7*, 2318–2328. https://doi.org/10.1101/gad.7.12a.2318

Stadler, H. S., Higgins, K. M., & Capecchi, M. R. (2001). Loss of Eph-receptor expression correlates with loss of cell adhesion and chondrogenic capacity in Hoxa13 mutant limbs. *Development*, *128*, 4177–4188.

Steichen-Gersdorf, E., Gassner, I., Superti-Furga, A., Ullmann, R., Stricker, S., Klopocki, E., & Mundlos, S. (2008). Triangular tibia with fibular aplasia associated with a microdeletion on 2q11.2 encompassing LAF4. *Clinical Genetics*, *74*, 560–565. https://doi.org/10.1111/j.1399-0004.2008.01050.x

Swinehart, I. T., Schlientz, A. J., Quintanilla, C. A., Mortlock, D. P., & Wellik, D. M. (2013). Hox11 genes are required for regional patterning and integration of muscle, tendon and bone. *Development*, *140*, 4574–4582. https://doi.org/10.1242/dev.096693

Szeto, D. P., Rodriguez-Esteban, C., Ryan, A. K., O'Connell, S. M., Liu, F., Kioussi, C., … Rosenfeld, M. G. (1999). Role of the Bicoid-related homeodomain factor Pitx1 in specifying hindlimb morphogenesis and pituitary development. *Genes & Development*, *13*, 484–494. https://doi.org/10.1101/gad.13.4.484

Uchihashi, T., Kimata, M., Tachikawa, K., Koshimizu, T., Okada, T., Ihara-Watanabe, M., … Michigami, T. (2007). Involvement of nuclear factor I transcription/replication factor in the early stage of chondrocytic differentiation. *Bone*, *41*, 1025–1035. https://doi.org/10.1016/j.bone.2007.08.028

Vanhoutteghem, A., Maciejewski-Duval, A., Bouche, C., Delhomme, B., Herve, F., Daubigney, F., … Djian, P. (2009). Basonuclin 2 has a function in the multiplication of embryonic craniofacial mesenchymal cells and is orthologous to disco proteins. *Proceedings of the National Academy of Sciences of the United States of America*, *106*, 14432–14437. https://doi.org/10.1073/pnas.0905840106

Visel, A., Minovitsky, S., Dubchak, I., & Pennacchio, L. A. (2007). VISTA enhancer browser–a database of tissue-specific human enhancers. *Nucleic Acids Research*, *35*, D88–D92. https://doi.org/10.1093/nar/gkl822

Vokes, S. A., Ji, H., Wong, W. H., & McMahon, A. P. (2008). A genome-scale analysis of the cis-regulatory circuitry underlying sonic hedgehog-mediated patterning of the mammalian limb. *Genes & Development*, *22*, 2651–2663. https://doi.org/10.1101/gad.1693008

Yamamoto, M., Gotoh, Y., Tamura, K., Tanaka, M., Kawakami, A., Ide, H., & Kuroiwa, A. (1998). Coordinated expression of *Hoxa-11* and *Hoxa-13* during limb muscle patterning. *Development*, *125*, 1325–1335.

Yamamoto-Shiraishi, Y., Higuchi, H., Yamamoto, S., Hirano, M., & Kuroiwa, A. (2014). Etv1 and Ewsr1 cooperatively regulate limb mesenchymal Fgf10 expression in response to apical ectodermal ridge-derived fibroblast growth factor signal. *Developmental Biology*, *394*, 181–190. https://doi.org/10.1016/j.ydbio.2014.07.022

Yamamoto-Shiraishi, Y., & Kuroiwa, A. (2013). Wnt and BMP signaling cooperate with Hox in the control of Six2 expression in limb tendon precursor. *Developmental Biology*, *377*, 363–374. https://doi.org/10.1016/j.ydbio.2013.02.023

Ye, W., Song, Y., Huang, Z., Osterwalder, M., Ljubojevic, A., Xu, J., … Chen, Y. (2016). A unique stylopod patterning mechanism by Shox2-controlled osteogenesis. *Development*, *143*, 2548–2560. https://doi.org/10.1242/dev.138750

Yokouchi, Y., Nakazato, S., Yamamoto, M., Goto, Y., Kameda, T., Iba, H., & Kuroiwa, A. (1995). Misexpression of Hoxa-13 induces cartilage homeotic transformation and changes cell adhesiveness in chick limb buds. *Genes & Development*, *9*, 2509–2522. https://doi.org/10.1101/gad.9.20.2509

Yokouchi, Y., Sasaki, H., & Kuroiwa, A. (1991). Homeobox gene expression correlated with the bifurcation process of limb cartilage development. *Nature*, *353*, 443–445. https://doi.org/10.1038/353443a0

Yue, F., Cheng, Y., Breschi, A., Vierstra, J., Wu, W., Ryba, T., … Ren, B. (2014). A comparative encyclopedia of DNA elements in the mouse genome. *Nature*, *515*, 355–364. https://doi.org/10.1038/nature13992

Zakany, J., Fromental-Ramain, C., Warot, X., & Duboule, D. (1997). Regulation of number and size of digits by posterior Hox genes: A dose-dependent mechanism with potential evolutionary implications. *Proceedings of the National Academy of Sciences of the United States of America*, *94*, 13695–13700. https://doi.org/10.1073/pnas.94.25.13695

Zakany, J., Zacchetti, G., & Duboule, D. (2007). Interactions between HOXD and Gli3 genes control the limb apical ectodermal ridge via Fgf10. *Developmental Biology*, *306*, 883–893. https://doi.org/10.1016/j.ydbio.2007.03.517

Zandvakili, A., & Gebelein, B. (2016). Mechanisms of specificity for Hox factor activity. *Journal of Developmental Biology*, *4*, 16. https://doi.org/10.3390/jdb4020016

Zhang, Y., Liu, T., Meyer, C. A., Eeckhoute, J., Johnson, D. S., Bernstein, B. E., … Liu, X. S. (2008). Model-based analysis of ChIP-Seq (MACS). *Genome Biology*, *9*, R137. https://doi.org/10.1186/gb-2008-9-9-r137

SUPPORTING INFORMATION

Additional supporting information may be found online in the Supporting Information section at the end of the article.